DOI: 10.1016/j.ijpharm.2021.121421

**Impact of blend properties and process variables on the blending performance.**

**Authors**

B.Bekaert[a], W. Grymonpré[b], A. Novikova[c], C. Vervaet[a], V. Vanhoorne[a]

[a]Laboratory of Pharmaceutical Technology, Department of Pharmaceutics, Ghent University, Ottergemsesteenweg 460, B-9000 Ghent, Belgium

[b]Fette Compacting Belgium, Schaliënhoevedreef 1 b, B-2800 Mechelen, Belgium

[c]Fette Compacting GmbH, Grabauer Str. 24, 21493 Schwarzenbek, Germany

*Corresponding author:

Institution: Laboratory of Pharmaceutical Technology

Address: Ghent University, Ottergemsesteenweg 460, B-9000, Ghent, Belgium

Tel: 0032 9 264 8118

Fax: 0032 9 264 8118

e-mail: valerie.vanhoorne@ugent.be

**Abstract**

In this study, quantitative relationships were established between blend properties, process settings and blending responses via multivariate data-analysis. Four divergent binary blends were composed in three different ratios and processed at various throughputs and impeller speeds. Additionally, different impeller configurations were tested to see their impact on the overall blending performance. During each run, feeder mass flows were compared with the API concentration (BU) in order to investigate the dampening potential of the blender. The blender hold-up mass (HM), mean residence time (MRT), strain on the powder (#BP) and BU variability ($RSD_{BU}$) were determined as blending descriptors and analyzed via PLS-regression. This elucidated the correlation between process settings (i.e. throughput and impeller speed) and blending responses, as well as the impact of blend properties on MRT and $RSD_{BU}$. Furthermore, the study revealed that HM does not need to be in steady state conditions to assure a stable BU, while it became clear that long/large feeder deviations can only be dampened by the blender when using dedicated impeller configurations. Overall, this study demonstrated the generic application of the blender, while the developed PLS models could be used to predict the blender performance based on the blend properties.

**List of abbreviations**

| | |
|---|---|
| #BP | Number of blade passes/Strain |
| API | Active pharmaceutical ingredient |
| CDC | Continuous direct compression |
| C_P | Caffeine anhydrous powder |
| DCP | Emcompress AN DC/Dicalcium phosphate |
| DoE | Design of experiments |
| HM | Hold-up mass |
| LC | Label claim |
| LIW | Loss-in-weight |
| MCL100 | Microcelac® 100/Co-processed microcrystalline cellulose and lactose |
| MF | Mass flow |
| MPT_µ | Metoprolol tartrate micronized |
| MRT | Mean residence time |
| NIR | Near infrared |
| PAT | Process analytical technology |
| P_µ | Paracetamol micronized |
| P_DP | Paracetamol dense powder |
| P_Gr | Paracetamol granular |
| P_P | Paracetamol powder |
| PCA | Principle component analysis |
| Pgel | Pharmgel/Pregelatinized maize starch |
| PH101 | Avicel PH-101/Microcrystalline cellulose |
| PLS | Partial least squares |
| $Q^2$ | Prediction |
| $R^2Y$ | Goodness of fit |
| RMSEcv | Root mean square error of cross validation |
| $RSD_{BU}$ | Relative standard deviation of the API concentration |
| RTD | Residence time distribution |
| T_P | Theophylline anhydrous powder |
| T80 | Tablettose 80/Lactose |

## 1 Introduction

In the last couple of years the aim of the pharmaceutical industry has shifted towards an increase in efficiency, flexibility and process knowledge (W. Engisch and Muzzio, 2015a; Van Snick et al., 2017b; Rogers et al., 2013). Furthermore, the pressure of generic drugs on the market urged the industry to pursue reduced developmental and manufacturing costs (Ierapetritou et al., 2016). A possible solution for these needs is a shift from batch to continuous manufacturing.

In the pharmaceutical industry, compression is a widely used production technique with an inherently continuous behavior. On the other hand, the unit operations preceding the compression step (i.e. weighing/feeding and blending) are usually performed batch-wise. To reach a full continuous direct compression line, these unit operations need to be integrated in a continuous manner. Recently, these requirements were met through the development of several innovative continuous direct compression (CDC) lines: ConsiGma™ CDC-50 by GEA Pharma Systems (2014); QbCon® by L.B. Bohle (2019); MODCOS by Glatt (2017); Fette Compacting Direct Compression Line by Fette Compacting GmbH (2016).

For each of these systems, continuous feeding is the first and most crucial step in order to maintain the correct mass balance during the manufacturing process (Simonaho et al., 2016). Any deviations during this unit operation will be passed down to the following process steps and can affect the final product quality (Ervasti et al., 2015; Van Snick et al., 2017b; Bostijn et al., 2019). Due to this criticality, extensive experimental work has been performed to investigate and optimize the feeding behavior of different raw materials (Engisch and Muzzio, 2014; Van Snick et al., 2019; Bostijn et al., 2019; Bekaert et al., 2021a). Still, feeders can transfer deviations in flow and blend composition to the subsequent blending/mixing unit operation. Most blending/mixing units are equipped to dampen deviations through the dilution of dosing errors in a larger powder volume. However, good radial and axial mixing is needed to dampen deviations and to ensure blend uniformity. Therefore, both experimental and modeling work has been performed, investigating the performance of continuous blenders as a function of material properties, process settings and blender configuration (Pernenkil and Cooney, 2006; Fogler, 2006; Marikh et al., 2006; Portillo et al., 2008; Gao et al., 2011; Osorio et al., 2016). A handful of papers also reported work on an integrated from-powder-to-tablet CDC line (Ervasti et al., 2015; Järvinen et al., 2013a; Järvinen et al., 2013b; Simonaho et al., 2016; Van Snick et al., 2017a; Van Snick et al., 2017b).

However, most of the published research was performed at lower throughputs ranging from 5 to 35 kg/h using a limited number of raw materials or focusing on a specific formulation. Furthermore, no in-depth research, investigating the dampening potential of the blender (i.e. ability of the blender to reduce or remove deviations), has been published. Therefore, the current paper aims to assess the processability of a wide range of binary blends at throughputs ranging from 5 to 80 kg/h on a blender designed for throughputs up to 200 kg/h. Four binary blends with different properties were processed to gain a better process understanding and to elucidate the impact of process and blender design variables on the blend quality and dampening potential. Additionally, a quantitative relationship between the blender performance as a function of blend properties and process settings was established via Partial Least Squares (PLS) regression.

## 2 Materials

An overview of the selected materials can be found in **Table 1,** including the supplier information and reference to the abbreviations used throughout the paper.

***Table 1:*** *Overview of selected materials*

| Material | Supplier | Code |
|---|---|---|
| Paracetamol powder | Mallinckrodt | P_P |
| Paracetamol dense powder | Mallinckrodt | P_DP |
| Paracetamol micronized | Mallinckrodt | P_µ |
| Paracetamol granular | Mallinckrodt | P_Gr |
| Caffeine anhydrous powder | Siegfried | C_P |
| Theophylline anhydrous powder | Siegfried | T_P |
| Metoprolol tartrate micronized | Utag | MPT_µ |
| Pearlitol 100 SD | Roquette | SD100 |
| Emcompress AN DC | JRS | DCP |
| Avicel PH-101 | FMC | PH101 |
| Tablettose 80 | Meggle | T80 |
| Microcelac® 100 | Meggle | MCL100 |
| Pharmgel | Cargill | Pgel |

## 3 Equipment

### 3.1 Continuous feeding and blending setup

A preliminary setup of a continuous direct compression line, without the lubricant blender and compression station, was used in this study (**Figure 1**). The setup consisted of material handling units, three loss-in-weight (LIW) feeders, a funnel, a linear tubular blender installed on top of an external catch scale, a conveyer belt, on-line process analytical technology (PAT) and a bin to collect the blended materials.

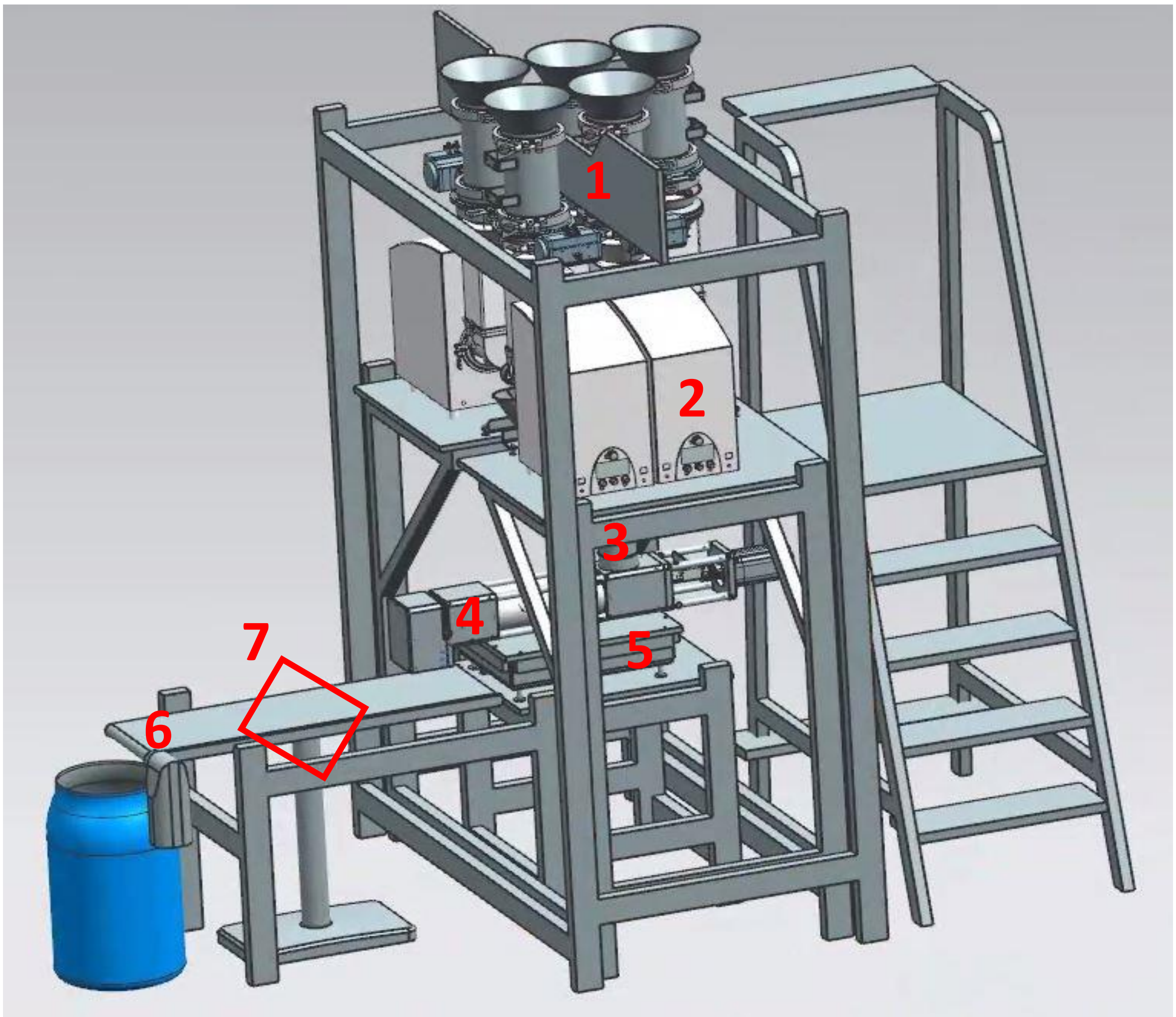


***Figure 1: Continuous feeding and blending setup*** *: (1) Material handling system; (2) LIW feeder platform; (3) funnel; (4) blender; (5) external catch scale; (6) conveyer belt; (7) position of PAT equipment. During this study, the LIW feeder platform was only equipped with 3 feeders.*

**3.1.1 Material handling and loss-in-weight feeding**

Material handling for each individual feeder was performed through a dedicated top-up system consisting of a conical hopper and a rotating butterfly valve (Fette Compacting Belgium, Mechelen, Belgium). Powder supply to the automated top-up systems was regulated via manual refills with prefilled powder bags.

Three Brabender DDSR20-HD loss-in-weight feeders (Brabender, Duisburg, Germany) were installed in staggered positions on a vibration-free platform. The central feeder, positioned above the inlet of the blending unit, was used for poorly flowing materials, reducing the possibility of powder adhesion to the funnel. Additionally, this feeder could be equipped with a high-frequency vibrator (Fette Compacting Belgium, Mechelen, Belgium) to improve the feeding performance of some challenging to feed materials (i.e. P_µ) (Bekaert et al., 2021). The third feeder was used for materials that could not reach the requested throughputs with a single feeder (i.e. high throughput runs with

P_µ). Brabender SMART Service (version DA 5.1.4.2) was used as the operating software (Brabender Technology, Duisburg, Germany). All feeder data (i.e. mass flow, net weight, hopper fill level, refill time and duration) was logged at 1s intervals. The software used for the data logging (i.e. FCDA - software) was provided by Fette Compacting (Schwarzenbek, Germany).

### 3.1.2 Blending unit

A symmetrical funnel with 60° angled slopes connected the feeders with the blender inlet. The prototype horizontal blender (Fette Compacting, Mechelen, Belgium) consisted of a tubular mixing chamber with a centrally rotating impeller. The impeller was a shaft equipped with a transport helix (i.e. length of 12 cm with a pitch of 4 cm) followed by 19 adjustable mixing paddles. For this study, the paddles were angled in a forward (i.e. +20°) and backward (i.e. -20°) direction, creating multiple (i.e. 4) turbulent mixing zones along the axis of the shaft, thus prolonging the axial back-mixing time in the blender. At the end of the shaft a single paddle was positioned perpendicular to the shaft. This standard impeller configuration is depicted in **Figure 2**. At the end of the blender, a weir plate could be installed consisting of a fixed semicircular plate combined with a movable semicircular plate. By moving the latter plate into different positions, the blender outlet could be 'fully closed' (0° position; impeding the main powder stream), partially closed (e.g. 30° position) or open (180° position)(**Figure 3**). Furthermore, the blender was placed on top of a loadcell (Mettler Toledo PBK987-CC300, Mettler-Toledo, Zaventem, Belgium) recording the hold-up mass at a frequency of 91.5 Hz. At the outlet, the blend was collected on a moving conveyer belt providing a continuous flow of material to the on-line near infrared (NIR) spectroscopy probe (SentroPAT FO, Sentronic, Dresden, Germany) mounted above the conveyer belt. Spectra were collected every second.

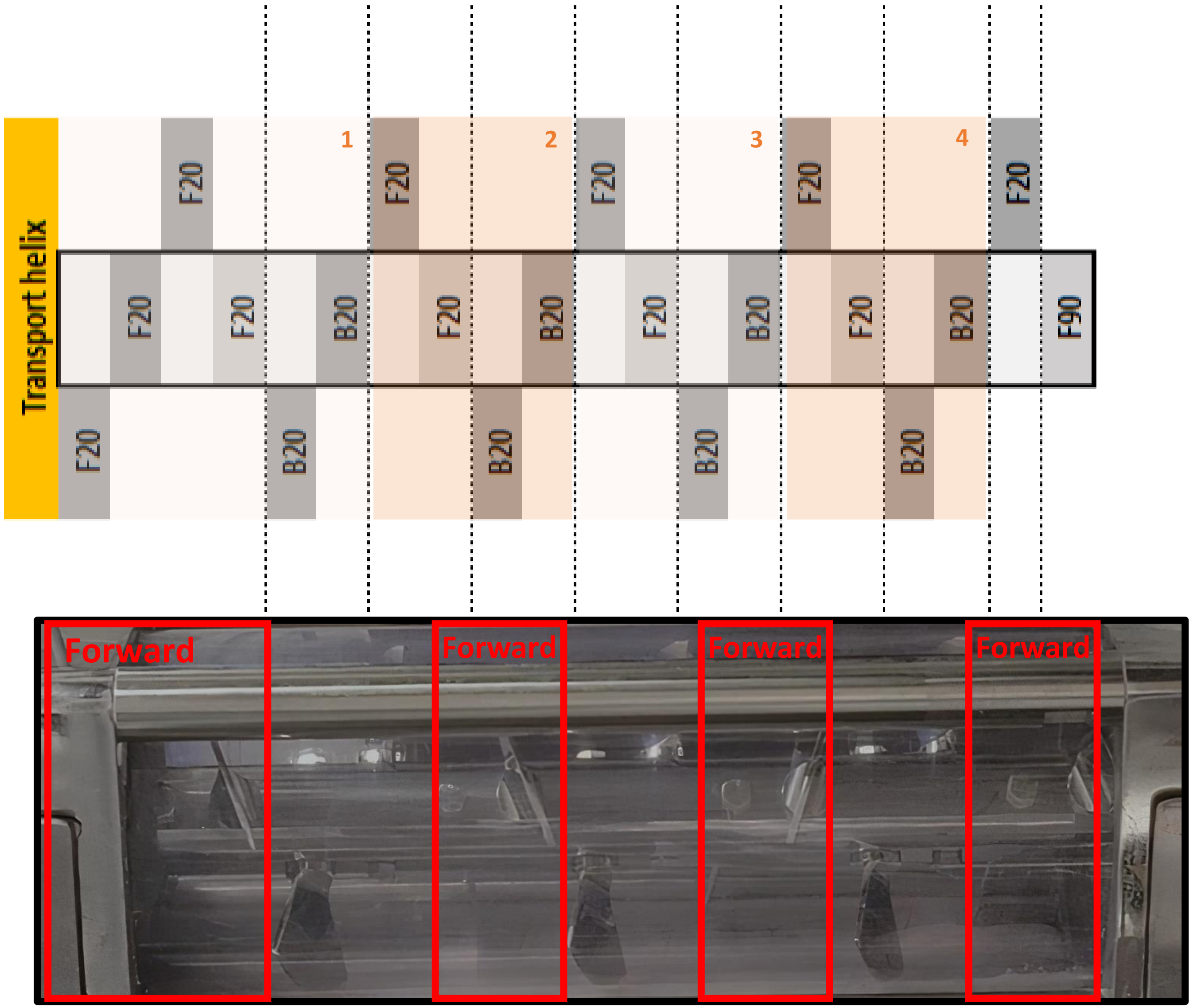


***Figure 2:*** *Schematic overview (top) and image (bottom) of the standard impeller configuration. The paddles were named according to their angle and direction (i.e. F20 = forward pushing with an angle of 20°; B20 = backward pushing with an angle of 20°) with the final paddle being perpendicular to the axis. Turbulent mixing zones are marked and numbered in orange.*

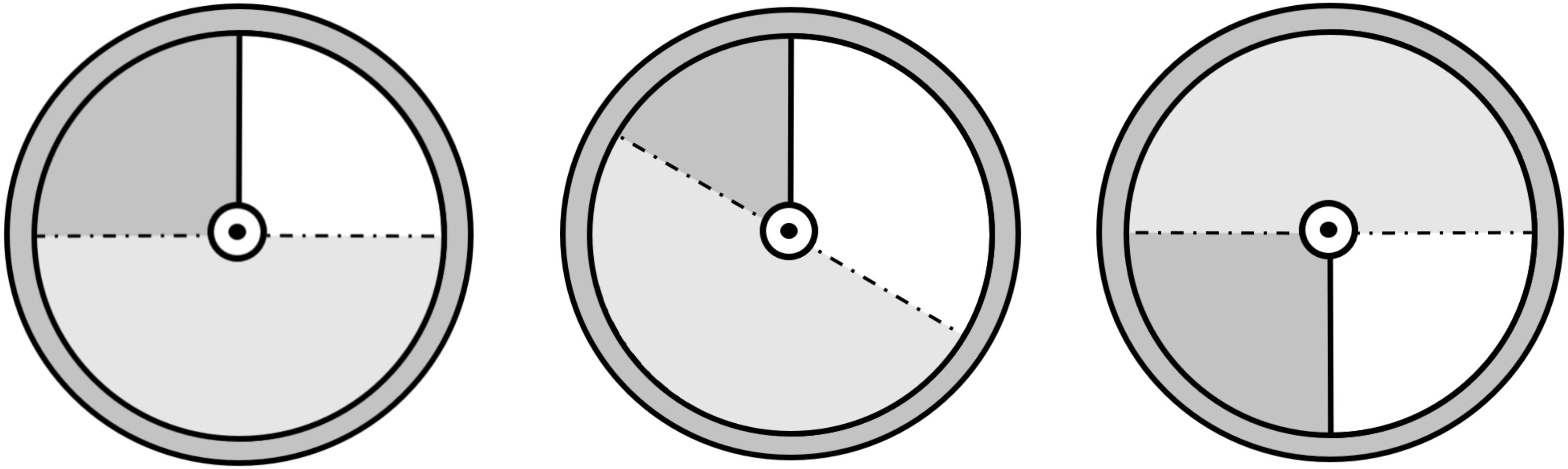

***Figure 3:*** *Front view of the weir plate with the different positions of the movable weir (light gray) used during the preliminary trials: (left) 0° or 'closed'; (middle) 30°; (right) 180° or open.*

### 3.2 Dynamic calibration setup

To develop the dynamic NIR API concentration models, an off-line test rig (Fette Compacting Belgium, Mechelen, Belgium) was constructed. The test rig consisted of a rotating circular table which can also move in a horizontal direction (**Figure 4)**. To present the material to the NIR probe (i.e. SentroPAT FO) a layer of material was placed on the table by pouring the material in the channel at the edge of the table. As the material was manually poured into this channel, the randomly induced variable distance between the powder bed and the probe and the variability in powder layer density allowed a dynamic presentation of the material when the table rotated in combination with its horizontal movement. Similar conditions will be encountered during NIR measurements of powder blends on the conveyor belt, therefore increasing the robustness of the models. Furthermore, the rotational speed of the table was adjusted to ensure an identical powder moving speed as on the conveyer belt used during the experimental runs.

***Figure 4:*** *(a) Off-line test rig used for the dynamic calibration and (b) movement of the test rig during a measurement with: (1) rotating and movable table; (2) channel with material; (3) NIR probe position.*

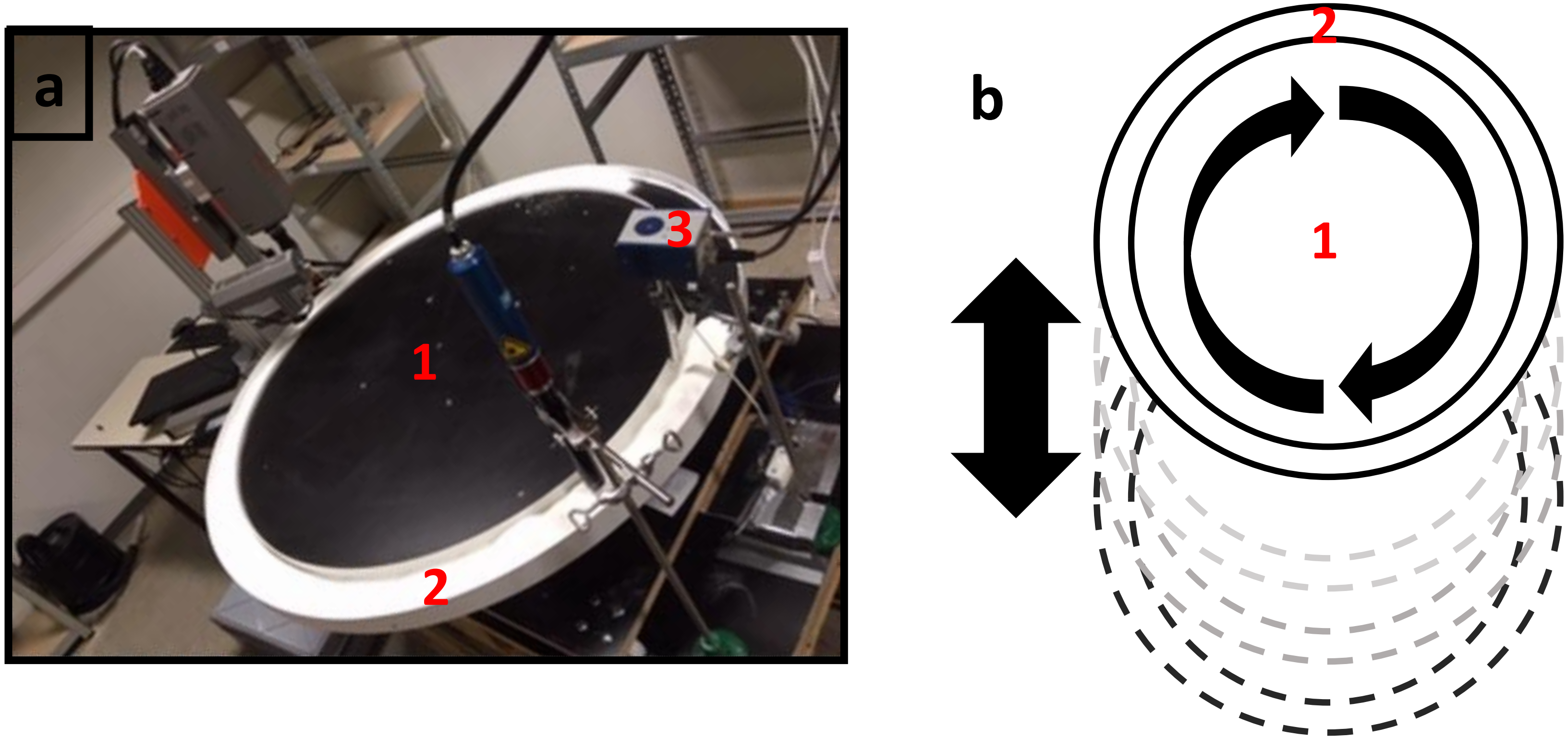

## 4 Methods

### 4.1 Blend characterization

Nine API-filler combinations were tested using three API ratios (i.e. 5%, 10% and 70%) resulting in a total of 27 blends. The blend composition was selected based on the raw materials used for the DDSR20-HD feeder characterization performed in an earlier study (Bekaert et al., 2021). The 27 blends were characterized for a set of descriptors that are potentially relevant during the blending process: compressibility, permeability, density, flowability, cohesion, porosity and wall friction. The protocols used for the blend characterization are based on the protocols described by Van Snick et al. (2018). A list of the descriptors, their abbreviations and applied characterization methods can be found in **Table 2**.

### 4.2 Blend selection

Principal Component Analysis (PCA) was performed in order to select blends with divergent properties. An overview of the analyzed blends is given in **Table 3**. Based on the results from the feeder trials performed by Bekaert et al. (2021), blends containing materials that could not reach the requested feeder throughputs (i.e. capacity limit using 1 API feeder) for the blender trials and/or were unable to achieve a stable mass flow throughout the process due to refill or bridging issues (i.e. caffeine anhydrous powder, Pharmgel and micronized metoprolol tartrate) were excluded. **Table 4** displays the selected blends.

### 4.3 Dynamic NIR API concentration models

Using the off-line test rig, dynamic PLS regression models were constructed for quantitative monitoring of the API concentration of the selected binary blends. The models were developed by regressing off-line collected and pre-processed NIR spectra with their corresponding API concentration level (i.e. 4, 5, 6, 7.5, 10, 12.5, 15, 65, 67.5, 70, 72.5 or 75%). Every second a spectrum was collected in the spectral region from 1100 to 2200 nm. Each collected spectrum was the average of 10 scans with a 7 ms integration time. The data was analyzed using The Unscrambler X software (Camo analytics, Oslo, Norway).

***Table 2:*** *Overview of blend descriptors, their respective abbreviation and applied characterization method.*

| Characterization method | Descriptor | Abbreviation |
|---|---|---|
| Flowpro | Flow through an orifice (= Flowrate) | FP |
| FT4 powder rheometer | Compressibility (at 15 kPa) | C_15kPa |
| | Permeability at 15 kPa | k_15kPa |
| Helium pycnometry | True density, porosity | $\rho$true, $\varepsilon$ |
| Tapping device | Bulk and tapped density | $\rho$b, $\rho$t |
| | Hausner ratio | HR |
| | Carr Index | CI |
| Ring shear tester | Angle of internal friction, angle of internal friction steady state flow, effective angle of internal friction | $\phi$lin, $\phi$sf, $\phi$e |
| | Cohesion | $\tau$c |
| | Consolidated density-weighed flow | ffp |
| | Flow function coefficient, major principal stress, unconfined yield stress | ffc, MPS, UYS |
| | Wall friction angle | WFA_S |

***Table 3:*** *Overview of characterized binary blends.*

| Name | API | Filler |
|---|---|---|
| **F1** | P_P | PH101 |
| **F2** | P_DP | DCP |
| **F3** | P_μ | DCP |
| **F4** | MPT_μ | SD100 |
| **F5** | C_P | T80 |
| **F6** | C_P | SD100 |
| **F7** | P_Gr | Pgel |
| **F8** | T_P | MCL 100 |
| **F9** | T_P | T80 |

***Table 4:*** *Overview of blends used during the blender trials and the $R^2Y$, #PC and RMSEcv from their corresponding dynamic calibration models.*

| Name | API | Filler | API% | $R^2Y$ | #PC | RMSEcv |
|---|---|---|---|---|---|---|
| | | | **F1** | | | |
| **F1_5** | | | 5 | 86.1 | 2 | 0.75 |
| **F1_10** | P_P | PH101 | 10 | 95.0 | 1 | 0.87 |
| **F1_70** | | | 70 | 86.8 | 2 | 1.21 |
| | | | **F2** | | | |
| **F2_5** | | | 5 | 87.1 | 3 | 0.81 |
| **F2_10** | P_DP | DCP | 10 | 95.0 | 1 | 0.80 |
| **F2_70** | | | 70 | 89.4 | 1 | 1.14 |
| | | | **F3** | | | |
| **F3_5** | | | 5 | 89.7 | 1 | 0.68 |
| **F3_10** | P_μ | DCP | 10 | 96.2 | 1 | 0.69 |
| **F3_70** | | | 70 | 90.2 | 1 | 1.05 |
| | | | **F9** | | | |
| **F9_5** | | | 5 | 76.0 | 1 | 1.04 |
| **F9_10** | T_P | T80 | 10 | 91.4 | 1 | 0.90 |
| **F9_70** | | | 70 | 91.5 | 1 | 1.03 |

### 4.4 Blending responses

#### 4.4.1 HM

The blender was installed on top of a loadcell that continuously monitored the hold-up mass at a frequency of 91.5 Hz.

#### 4.4.2 MRT and #BP

MRT and #BP were calculated from the residence time distribution (RTD) estimation. RTD was estimated by performing a spike test during steady state conditions (i.e. < 2g change in hold-up mass over 1 minute). A small spike of sodium saccharin (i.e. 5% of the actual blender hold-up mass) was introduced instantaneously into the blender inlet and monitored as a function of time via NIR-measurement at the blender outlet (i.e. Sentronic probe installed above the transport belt). The spike amount was chosen such that it was detectable by the NIR system but did not disturb the flow behavior of the blend. The absorbance of the measured spike as a function of time resulted in an absorbance profile, i.e. a(t). This curve was used to calculate the RTD function e(t) using **Equation 1**.

$$e(t) = \frac{a(t)}{\int_0^\infty a(t)dt} \qquad \textbf{(Eq.1)}$$

The mean residence time (MRT) was calculated from the RTD function e(t) using **Equation 2** (Fogler, 2006)**:**

$$MRT = \frac{\int_0^\infty t\, e(t)dt}{\int_0^\infty e(t)dt} \qquad \textbf{(Eq.2)}$$

To determine the number of blade passes (#BP), MRT and impeller speed were required to solve **Equation 3**:

$$\#BP = MRT\ x\ \frac{Impeller\ speed\ (rpm)}{60} \qquad \textbf{(Eq.3)}$$

#### 4.4.3 API concentration variability

During the experiments, NIR spectra of the blends were collected every second by the Sentronic probe, positioned at the outlet of the blender. The NIR probe had a spot size of 6 mm (experimentally verified) with a maximum penetration depth of 0.5 mm. The collected NIR spectra were loaded into the developed BU calibration models (i.e. PLS models) in order to predict the API concentration over time. Due to a variable sample presentation (i.e. variable height of the powder layer on the conveyer belt), the total number of averaged spectra was chosen to equal an average sample size of 200 mg which is in the same order as a unit dose (i.e. single tablet). Using **Equation 4**, the variability of the API concentration over an entire blender run was calculated:

$$RSD_{BU} = \frac{Standard\ deviation\ (BU)}{Mean\ (BU)}\ x\ 100 \qquad \textbf{(Eq.4)}$$

### 4.5 Weir plate trials

The impact of the weir plate on the blending process was determined by performing a full-factorial experimental screening design with throughput, impeller speed and weir plate angle as factors. The throughput was set at 5, 42.5 and 80 kg/h. The impeller speed was set at a Froude number of 2 (i.e. 173 rpm), 5 (i.e. 274 rpm) and 8 (i.e. 346 rpm) (Zeki Berk, 2009). The angle of the weir plate was tested at 0° ('closed'; restricting normal powder flow), 30° and 180° (open blender outlet) (**Figure 3**). The impeller configuration (i.e. standard configuration; **Figure 2**) and API ratio (i.e. 10%) remained fixed during this experimental design. Furthermore, the experiments were done for two of the selected binary blends (i.e. F1 and F9) in order to determine a potential blend interaction. F1 was chosen as a blend where its cohesive properties could affect the blending performance, while F9 was selected as a model blend with intermediary properties. The investigated responses were HM, MRT, #BP and $RSD_{BU}$.

MODDE 12 software (Umetrics, Umeå, Sweden) was used to regress the responses against the factors via multiple linear regression (MLR). The factors were pre-treated prior to MLR via orthogonal scaling and centering. Each effect was calculated with 95% confidence intervals in order to evaluate the significance of factors and factor interactions.

### 4.6 Blender trials

Blender trials were performed in order to characterize the inherent blending performance of the blender for the selected binary blends, as well as finding a quantitative relationship between the blender performance and the blend properties and process settings.

#### 4.6.1 Experimental setup

The impact of varying blend compositions and process settings was investigated according to a full factorial DoE with throughput (i.e. 5, 42.5 and 80 kg/h), impeller speed (i.e. Froude number 2, 5 and 8), API concentration (i.e. 5, 10 and 70%) and blend properties (i.e. t1 and t2) as factors. The blend properties were included as their principle component 1 (t1) and 2 (t2) scores (derived from the binary blend PCA model). While t1 described the flowability and compressibility of the blend, t2 represented differences in density and porosity. The impeller configuration (i.e. standard configuration without a weir plate) remained fixed during the trials. An overview of the full factorial DoE is given in **Table 5**.

Prior to start-up, the feeders were primed (i.e. running for 5 to 10 seconds at the required screw speed in order to fill the screws) and the blender tared. Next, the raw materials were fed individually into the blender in order to reach the requested throughput and API concentration. The feeding-blending process was run for 45 minutes assuring steady state conditions for the hold-up mass. After a runtime of 45 minutes, the feeders were stopped and the blender continued running until empty. Datalogging was performed by the feeder software (FCDA, Fette compacting, Schwarzenbek, Germany), blender loadcell (Mettler-Toledo, Zaventem, Belgium) and NIR probe (SentroPAT FO, Sentronic, Dresden, Germany).

***Table 5:*** *Overview of the factor settings of the full factorial DoE.*

| Name | Type | Settings |
|---|---|---|
| **Throughput (kg/h)** | Quantitative | 5 to 80 |
| **Froude** | Quantitative | 2 to 80 |
| **API% (%)** | Multilevel | 5; 10; 70 |
| **t1 (flow and compr)** | Quantitative | -7.84 to 7.84 |
| **t2 (density and porosity)** | Quantitative | -4.6 to 4.6 |

**4.6.2 Feeder responses**

During the blender trials, data logging of the feeders continuously monitored the amount of material fed to the blender. The internal loadcell of the feeders generated mass flow profiles from which the percentage label claim (LC) was calculated (**Eq.5**):

$$\mathrm{LC}\ (\%) = \frac{\text{mass flow (g/s)}}{\text{mass flow set point (g/s)}} \times 100 \qquad (\textbf{Eq.5})$$

These LC profiles were used to locate and quantify deviations during the feeding process (e.g. mass flow overshoots due to feeder refills or inconsistent screw filling of cohesive materials) that potentially could influence the quality of the blend. The quantification was done by fitting the LC profiles with a polynomial fit. The deviation between the LC profile and polynomial fit was plotted in function of time (i.e. residual plot) as displayed in **Figure 5**. From the residual plot, the duration ($Res_D$) and area under the curve ($Res_{AUC}$) (**Eq.6**) of the rectangle with equal area under the curve were calculated (Van Snick B, 2019; Bekaert et al., 2021):

$$Res_{AUC} = \int_{t\ start\ disturbance}^{t\ end\ disturbance} Residuals(t)dt \qquad \textbf{(Eq.6)}$$

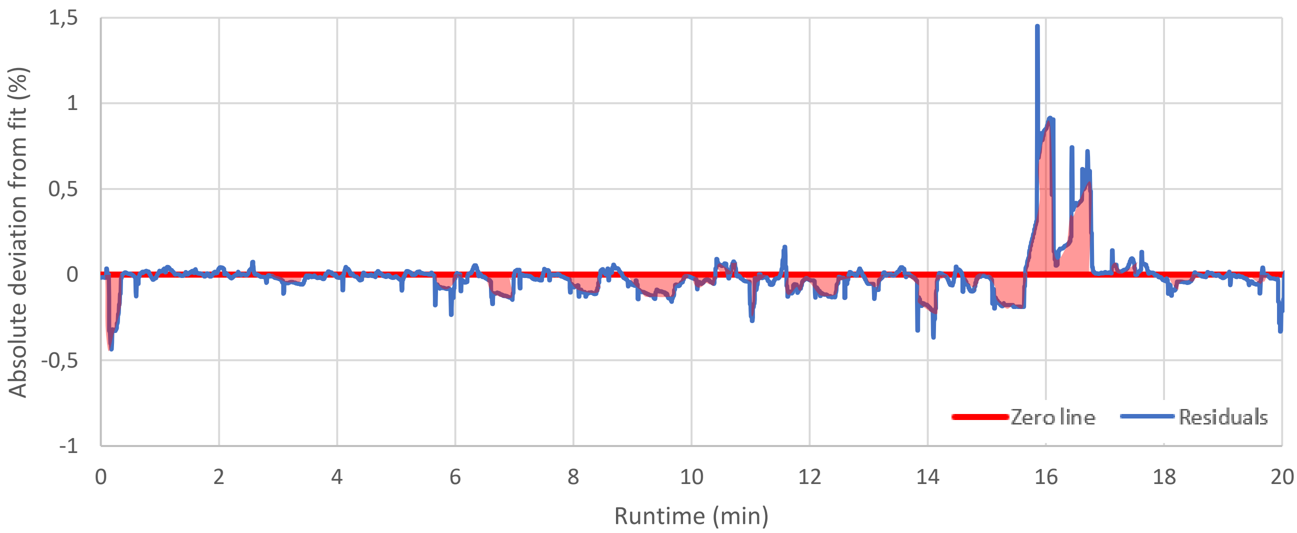


***Figure 5:*** *(a) Residual plot for the run with F1_5_1 (5% API; Thr of 42.5 kg/h; Fr 5). The AUC of the deviations is marked in red.*

#### 4.6.3 Blending responses

The continuous hold-up mass measurement was used to quantify (**Eq.6**) the deviations introduced by the blender (e.g. layering of the impeller or blender wall) or deviations passed down by the feeder (e.g. flushing of the feeder, refill overshoots or inability to reach the mass flow setpoint). Furthermore, the ability of the blender to reduce or remove these deviations (i.e. dampening potential) was determined by evaluating the propagation of the deviations along the feeding and blending process.

### 4.6.4 Residence time distribution

RTD experiments were performed using a spike of sodium saccharine, equivalent to 5% of the actual holdup mass. The spike was introduced during steady state conditions and monitored as a function of time via NIR spectroscopy at the blender outlet. MRT and #BP were calculated from the RTD experiments using **Equation 2** and **3**.

### 4.6.5 API concentration

NIR spectra were collected by the Sentronic probe at the outlet of the blender. The collected spectra were loaded into the developed BU calibration models (i.e. PLS models) in order to predict the API concentration over time. Additionally, the API concentration measurements were used as another method to determine the dampening potential of the blender through the comparison of the propagated hold-up mass deviation into the BU measurement.

For each experimental run, 20 grab samples were taken over a period of 5 minutes (i.e. 1 sample every 15 seconds). The grab samples were analyzed via UV-VIS analysis as an analytical reference method. 200 mg of blend (i.e. equal to a single tablet) was homogenized in 50 mL distilled water and diluted 1/50 . Next, the API content was determined using a UV spectrophotometer with a 1 cm cell (Shimadzu UV-1650PC, Shimadzu Corporation, Kyoto, Japan). The absorbance was measured at a wavelength of 243 nm for paracetamol blends (i.e. F1, F2 and F3) and 272 nm for the theophylline blend (i.e. F9). The reference concentrations obtained from the UV-VIS measurements were used as a verification of the API concentrations determined via on-line NIR spectroscopy.

### 4.6.6 Multivariate data analysis

MODDE 12 software (Umetrics, Umeå, Sweden) was used to regress the responses against the factors via multiple linear regression (MLR). The factors were pre-treated prior to MLR via orthogonal scaling and centering. Each effect was calculated with 95% confidence intervals in order to evaluate the significance of the factors and factor interactions.

One overall PLS model was developed where the blend properties and process parameters (X-matrix) were regressed versus the blending responses of the four selected binary blends (Y-matrix). The dataset was pre-treated prior to PLS regression via unit variance (UV) scaling and mean centering. Finally, log transformation was applied to non-normally distributed responses. SIMCA 16 software (Umetrics, Umeå, Sweden) was used to create the PLS model.

### 4.7 Impeller configuration evaluation

Five impeller configurations were screened during the blending process of one binary blend (i.e. F9) in order to assess the impact of the impeller configuration (i.e. changing paddle angles or adding/removing mixing zones) on the mixing performance (i.e. higher/lower $RSD_{BU}$), hold-up mass (i.e. material at risk) or the mean residence time (MRT) of the product. The screening was performed at a fixed throughput (i.e. 5 kg/h), impeller speed (i.e. Fr 8) and API ratio (i.e. 10%) and no weir plate was installed at the end of the impeller shaft. Additional tests were performed for impeller configuration 5 in order to determine the impeller speed sensitivity. During these tests, the impeller speed was varied in order to obtain Froude numbers between 2 and 16. An overview of the different impeller configurations and screening runs are depicted in **Figure 6** and **Table 6**, respectively.

***Table 6:*** *Overview screening runs for the impeller configuration evaluation and corresponding HM, MRT and $RSD_{BU}$.*

| Run# | Throughput (kg/h) | Froude | API% (%) | Impeller configuration | HM (g) | MRT (s) | $RSD_{BU}$ (%) |
|---|---|---|---|---|---|---|---|
| **1** | 5 | 8 | 10 | Standard | 155 | 80 | 7.60 |
| **2** | 5 | 8 | 10 | 2 | 160 | 78 | 6.60 |
| **3** | | | | 3 | 270 | 141 | 6.00 |
| **4** | | | | 4 | 160 | 11 | 8.50 |
| **5** | | | | 5 | 135 | 38 | 6.43 |
| **6** | 5 | 2 | 10 | 5 | 215 | 51 | 5.54 |
| **7** | 5 | 16 | 10 | 5 | 140 | 18 | 10.66 |

*__Figure 6:__ Overview of the different impeller configurations used during the preliminary tests. Light-grey colored paddles are positioned at the bottom of the impeller shaft. Turbulent mixing zones are marked and numbered in orange and changes in configuration compared to the standard configuration are marked in red.*

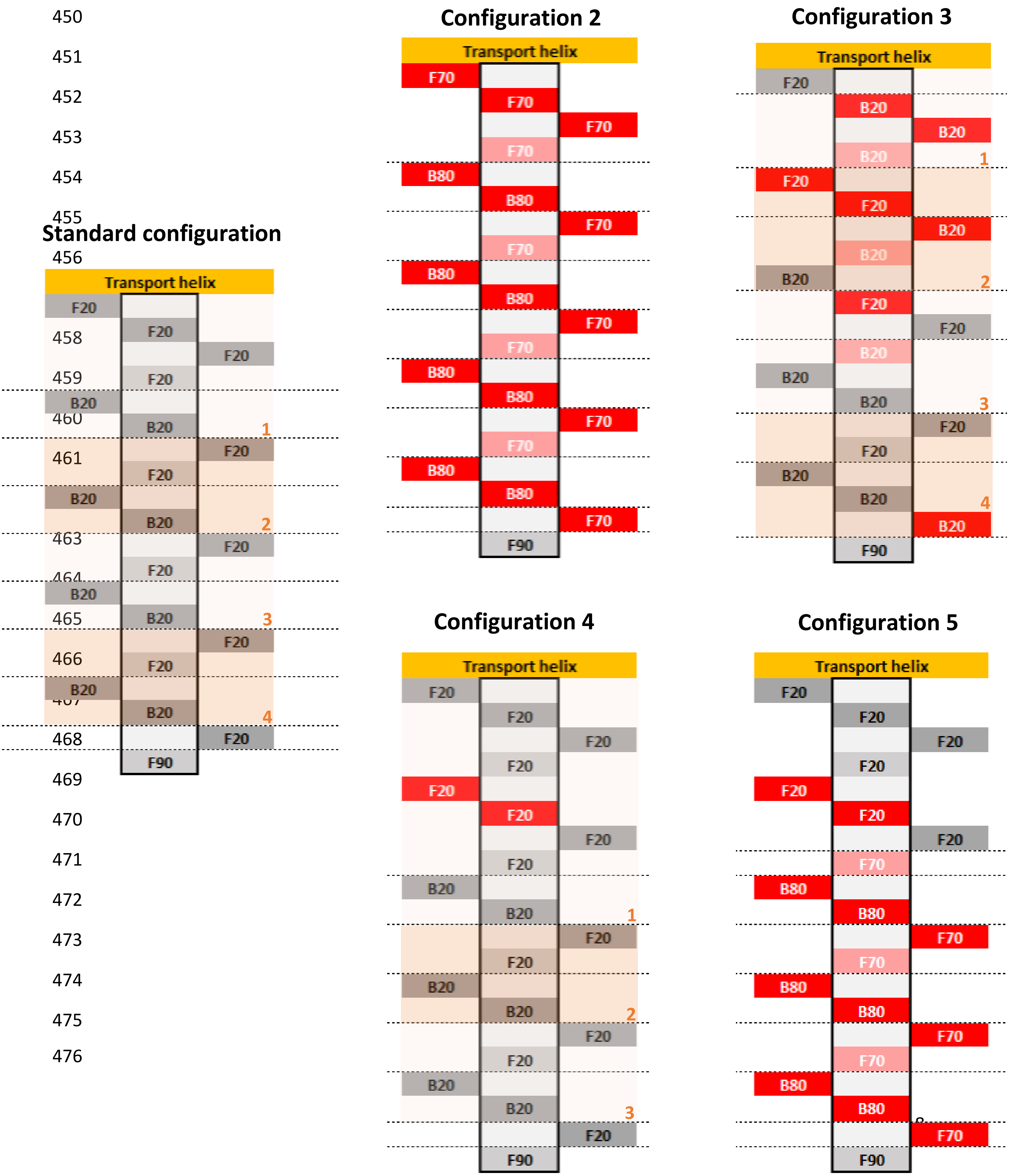

## 5 Results and discussion

### 5.1 Blend characterization and selection

Nine API-filler combinations in three API ratios (i.e. 27 blends) were characterized resulting in a PCA model with 3 principle components (PCs) and a goodness of fit ($R^2X$) and prediction ($Q^2$) of 82.3 % and 56.7%, respectively. The corresponding scores plot depicts the relationship of the different blends/blend ratios to each other based on their properties, whereas the loadings plot reveals the correlations between the different properties. Both plots are superimposable, meaning that blends with a specific location on the scores plot have high values for the properties on the same location in the loadings plot and low values for those at the opposite side of the origin. **Figure 7** shows the scores and loadings plots for PC1 vs. PC2. The scores plots showed cluster formation of specific blends. Firstly, the low API ratio blends (i.e. 5 and 10%) were clustered based on their filler properties, indicating their importance in low-dose drugs. Secondly, the 70% blends were clustered on the left side of the plot due to the intrinsic lower flowability of APIs, except for the highly dense APIs (i.e. P_DP and P_GR).

Taking the influence of all measured properties into consideration (i.e. multivariate screening), 12 blends (i.e. four blend compositions in three API ratios) with different physicochemical properties were selected in order to cover a wide variety of blends (**Table 4**). The first step was to select blends at the edges of the blend cluster: F1 (P_P + PH101), showing positive correlations with cohesivity and compressibility, was chosen to investigate the impact of highly compressible blends on the process. The location of F2 (P_DP + DCP) at the opposite side of the origin was mainly influenced by its highly flowable and dense components and was picked to investigate the blending performance of denser blends. F3 (P_µ + DCP), which combined a light and dense powder, showed shifts in blend properties for the different API ratios (i.e. going from highly cohesive to a dense and intermediate flowing blend). These shifts combined with the segregation potential were used to determine their effect on the processability. Finally, F9 (T_P + T80) located close to the origin of the PCA plot, was included as a blend with intermediate properties compared to the other blends. Furthermore, including the three API ratios into the selection generated a wide variety of blends along both PC1 and PC2.

504 505 ***Figure 7:*** *PC 1 vs PC 2 scores (a) and loadings (b) plot of the Blend PCA model. The naming in the scores plot consists of the blend name followed by the API concentration. Coloring was performed based on the API content. The cut-out colored the points according to their filler.*

506 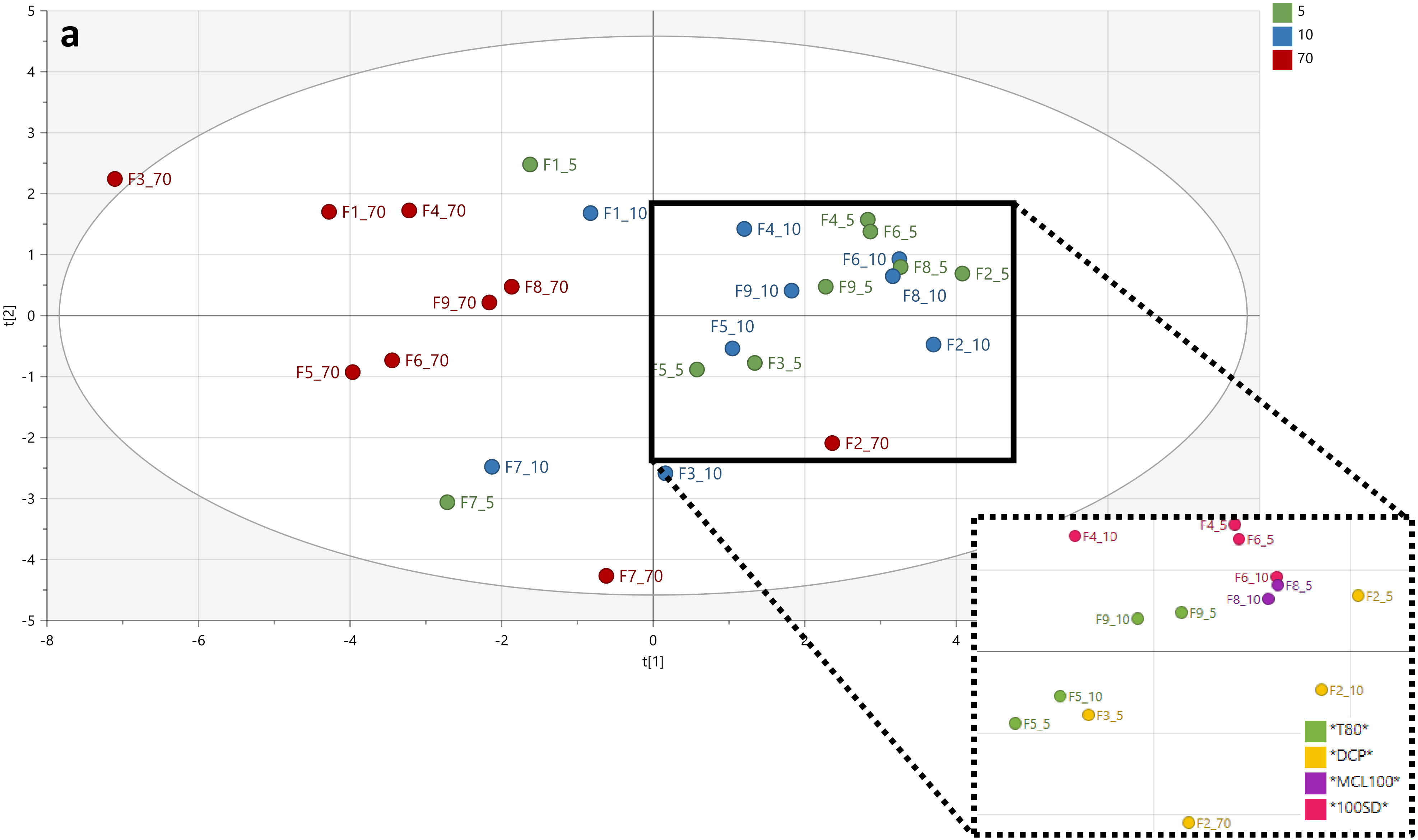

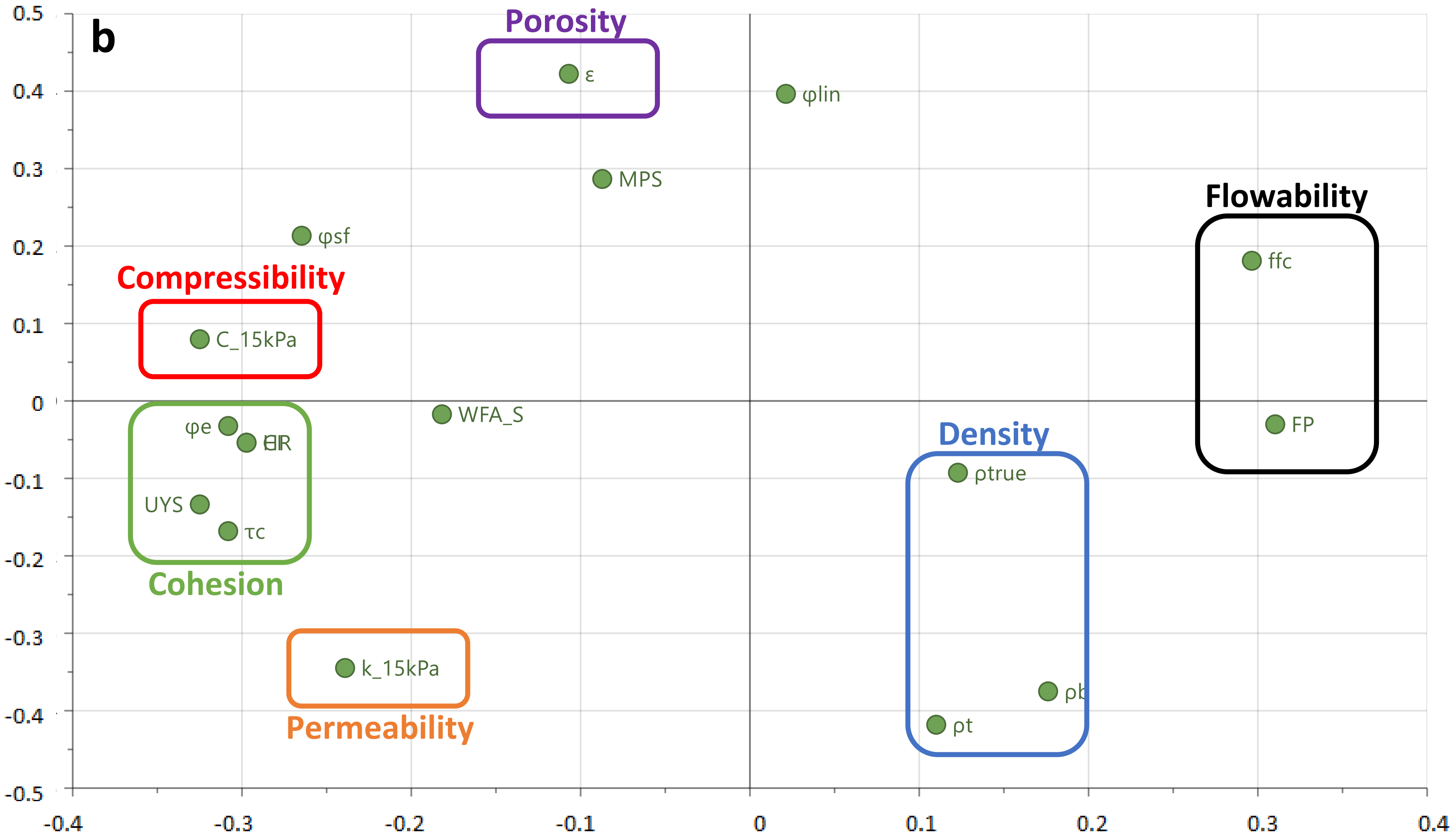
b
Porosity
ε
φlin
MPS
φsf
Compressibility
C_15kPa
Flowability
ffc
FP
WFA_S
φe
UYS
τc
Cohesion
Density
ρtrue
k_15kPa
Permeability
ρt
0.5
0.4
0.3
0.2
0.1
0
-0.1
-0.2
-0.3
-0.4
-0.5
-0.4
-0.3
-0.2
-0.1
0
0.1
0.2
0.3
0.4

### 5.2 Dynamic calibration models

**Table 4** displays an overview of the constructed calibration models with their goodness of fit ($R^2Y$), number of principle components (#PC) and prediction error (Root Mean Square Error of cross validation; RMSEcv). The full spectral region (i.e. 1100 to 2200 nm) was selected for analysis via PLS regression after standard normal variate (SNV) correction and mean centering. Standard cross validation was performed by dividing the dataset into 5 groups in order to calculate the RMSEcv of the model. Overall, the nature of the dynamic measurement (i.e. deliberately introducing density changes and differences in the distance between the powder bed and probe in order to improve the robustness of the prediction) induced a relatively high variability in the calibration spectra, reducing the predictive performance (i.e. higher RMSEcv).

### 5.3 Weir plate trials

In this experimental design the main focus was to determine the significance of a weir plate at the blender outlet, hence evaluating its potential to impact the blending process (i.e. dampening potential, HM, MRT, #BP). **Figure 8** depicts the coefficient plots for the different blender responses of F9 (similar results were obtained for F1). A coefficient plot displays the regression coefficients of each factor and factor interaction. The regression coefficient of a factor is the quantitative change in a specific response value when this factor increases from its average value to a higher level, while keeping the other factors at an average value. The coefficient plots showed that a change in weir plate angle had no significant influence on any blender response (i.e. 95% confidence interval of the regression coefficient includes zero). These results demonstrated that there is no significance in adding a weir plate to the blender.

The coefficient plots depicted a significant impact of throughput, Froude number and their interactions on the blender responses. An increase in throughput accrued more mass in the blender (i.e. higher HM), but also generated a pushing effect decreasing the residence time (MRT) of the material in the blender and reducing the number of blade passes. Furthermore, an increase in Froude number amplified the pushing effect by spinning the paddles faster, thus reducing MRT and HM. The influence of the throughput-Froude number interaction on HM was governed by the Froude number due to the larger changes in HM when varying the Froude number compared to the throughput.

***Figure 8: Weir plate DOE:*** *Coefficient plots for each blending response (i.e. HM, MRT, $RSD_{BU}$ and #BP) for F9. Significance was determined using a 95% confidence interval.*

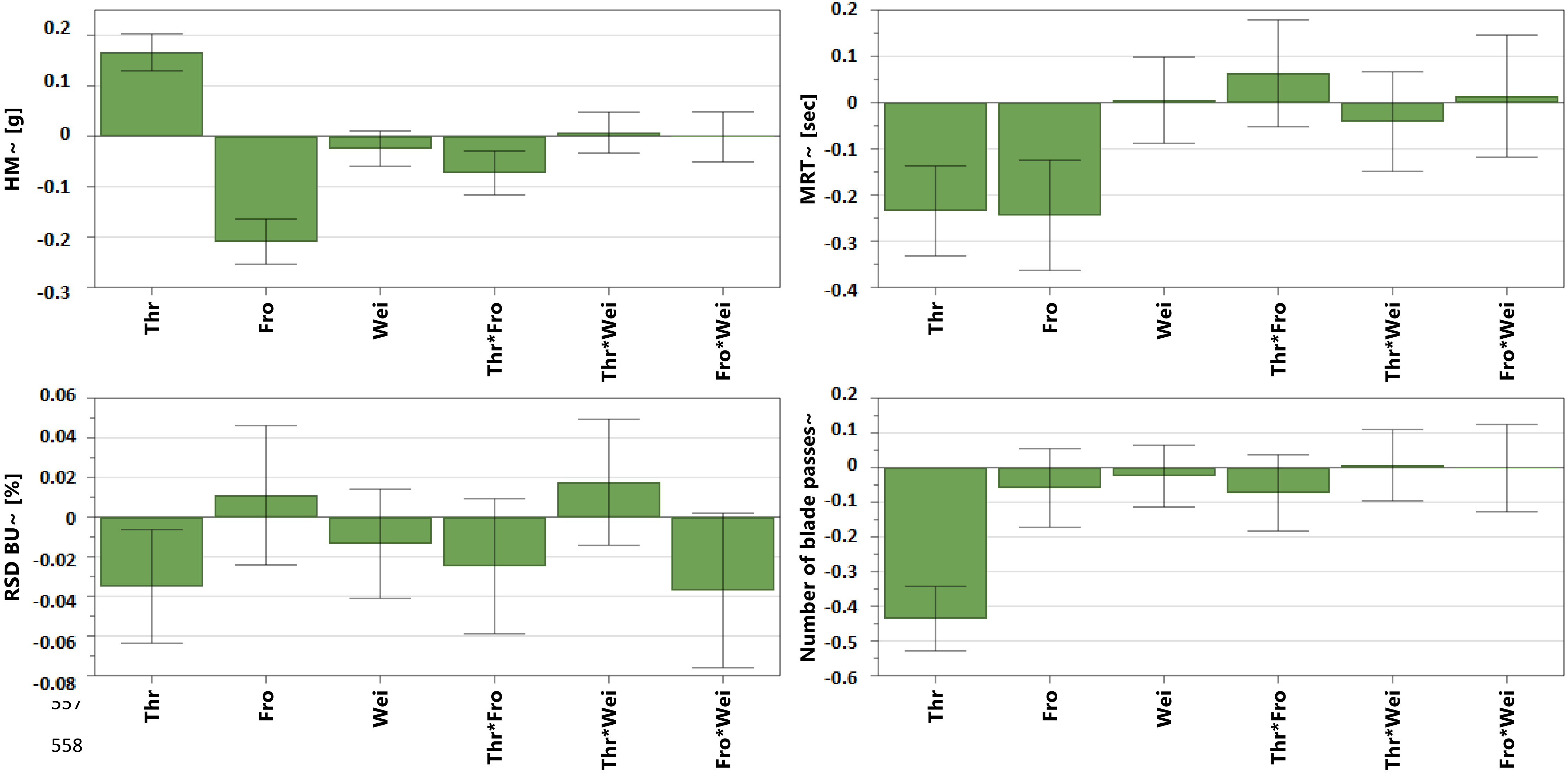

### 5.4 Blender trials

#### 5.4.1 Blender performance

The blender trials were performed on a generic blender with the standard impeller configuration, as depicted in **Figure 6**, without the weir plate. The trials allowed to determine the overall blender performance by investigating the dampening potential (i.e. reduce/remove deviations) and the time needed to reach steady state for both HM and BU. Furthermore, a quantitative relationship between the blender performance as a function of blend properties and process settings was developed.

##### 5.4.1.1 Dampening potential

The dampening potential was evaluated by comparing the label claim profiles from the feeders (taking the mass flow from both API and filler feeders into consideration) with the blender hold-up mass and API concentration in order to detect how a deviation propagated through the line. **Figure 9a** displays several deviations from the setpoint (i.e. label claim deviations) originating from the API feeder for F1 (i.e. P_P and PH101) at a throughput of 5 kg/h and Fr 2. Next to the short-term deviations (i.e. < 30 seconds), a significant deviation was observed for a longer period of time on three occasions. These were most likely caused by the non-optimized feeder control settings for all materials (i.e. default parameter list was used since this was not the scope of this study) having difficulties coping with sudden densifications in the powder bed (e.g. breakage of bridge/rathole; drop of powder during refill) and could have a significant influence on the API percentage in the final blend (Bekaert et al., 2021). The blender hold-up mass (**Figure 9b**) also captured the first two deviations captured by the blender, while the third one (i.e. shorter and smaller deviation) was reduced drastically. Additionally, two new peaks were seen in the hold-up mass which were caused by the spike tests for the blender RTD measurements (i.e. first = color spike; second = API spike). Furthermore, the short-term feeder deviations were removed completely by the blender, demonstrating its dampening potential. Looking at the BU profile (**Figure 9c**), the same peaks as in the blender were observed after a small delay (i.e. equal to the MRT), confirming the inability of the current blender configuration to dampen the observed longer term feeder fluctuations.

***Figure 9:*** *Data from the experimental run F1_5_2 (i.e. 5% P_P at a throughput of 5 kg/h and Froude 2). The profiles describe the deviation from setpoint for: (a) API label claim, taking the mass flow from both API and filler feeders into consideration ; (b) hold-up mass from blender loadcell; (c) API concentration measured by the Sentronic probe. Significant deviations are marked with a red arrow. The color and API spike for the RTD measurement were captured by the blender loadcell (marked with a black arrow). The API spike was also captured by the NIR probe (marked with a black arrow).*

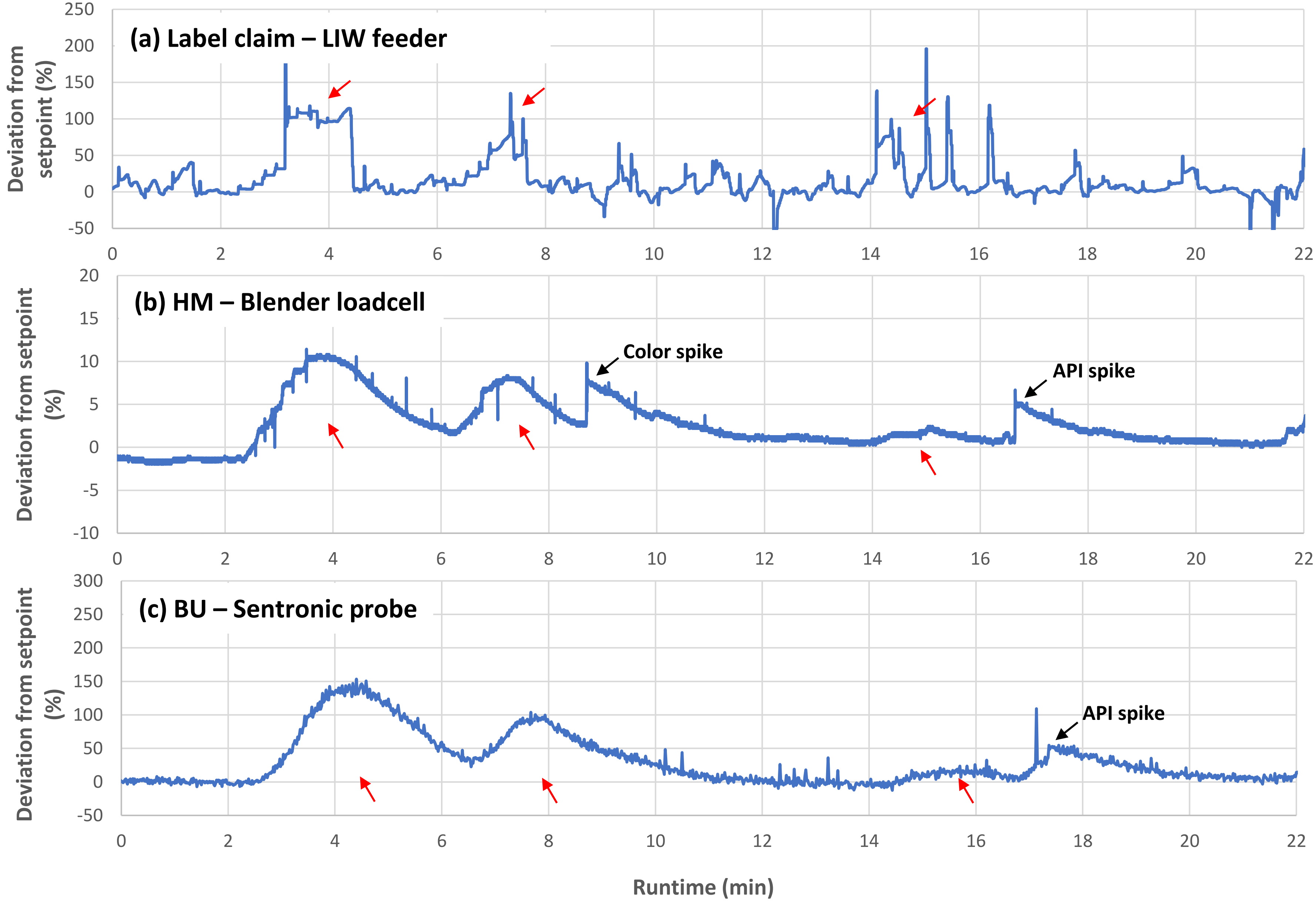

At higher throughput runs with F1 (i.e. 42.5 and 80 kg/h), multiple refills were initiated by the feeders during which the addition of fresh material induced an initial flushing effect (i.e. instantaneous stream of powder leaving the feeder) combined with densification of the powder (i.e. more screw filling). These phenomena generated overshoots in the mass flow which were detected by the blender loadcell (**Figure 10**). Based on the area under the curve of the refill overshoot signal these were highly consistent (**Table 7**), with only small deviations (defined by an AUC between -1 and 1 %.min) related to the variability in powder volume added by the top-up system. Furthermore, the API concentration profile showed no visible peaks, suggesting the blender was able to cope with these small deviations.

The abovementioned observations were applicable for all formulations suggesting that depending on the extent of the deviations introduced by the feeder, the blender was able to sufficiently dampen or even remove short-term deviations. However, the current impeller configuration did not allow the blender to reduce/remove larger and longer-term deviations, which are defined as feeder deviations resulting in a blender hold-up mass deviation larger than 5% for more than 30 seconds. In case the feeding process could not be optimized, a change in impeller configuration, as proven in **Section 5.5**, could be a potential solution.

The blender trial tests also suggested that the blender loadcell could be used as a soft sensor in order to get high-level feedback on potentially relevant deviations as well as provide information on the refill consistency.

***Table 7:*** *Refill consistency: ResAUC calculated for the overshoots observed during the main blender trial runs for F1_5_6 (Figure 10; 5% P_P; 80 kg/h, Fr 5); F1_10_7 (10% P_P, 80 kg/h, Fr 8); F9_5_6 (5% T_P, 80 kg/h, Fr 5); F9_10_7 (10% T_P, 80 kg/h, Fr 8).*

| | $Res_{AUC}$ (%.min) | | | |
|---|---|---|---|---|
| **#Overshoot** | **F1_5_6** | **F1_10_7** | **F9_5_6** | **F9_10_7** |
| **1** | 0.0052 | 0.003 | 0.0246 | 0.0164 |
| **2** | 0.0054 | 0.0028 | 0.0202 | 0.0204 |
| **3** | 0.0046 | 0.0025 | 0.0214 | 0.0181 |
| **4** | 0.0049 | 0.0025 | 0.024 | 0.0197 |
| **5** | 0.0053 | 0.0029 | 0.0242 | 0.0168 |
| **6** | 0.005 | 0.0032 | 0.0231 | 0.0173 |
| **7** | 0.0044 | 0.0031 | 0.0237 | |
| **8** | 0.0043 | 0.0032 | 0.022 | |
| **9** | 0.0043 | 0.0027 | | |
| **10** | 0.0049 | | | |
| **11** | 0.005 | | | |
| **12** | 0.0043 | | | |
| **Mean** | **0.0048** | **0.0029** | **0.0229** | **0.0181** |
| **RSD** | **8.474** | **9.481** | **6.769** | **8.924** |

***Figure 10***: *(a) Visualization of the mass flow overshoots, occurring every refill, for run F1_5_6 (i.e. 5% P_P at a throughput of 80 kg/h and Froude 5); (b) Corresponding profile displaying deviation from the API concentration target (i.e. 5%).*

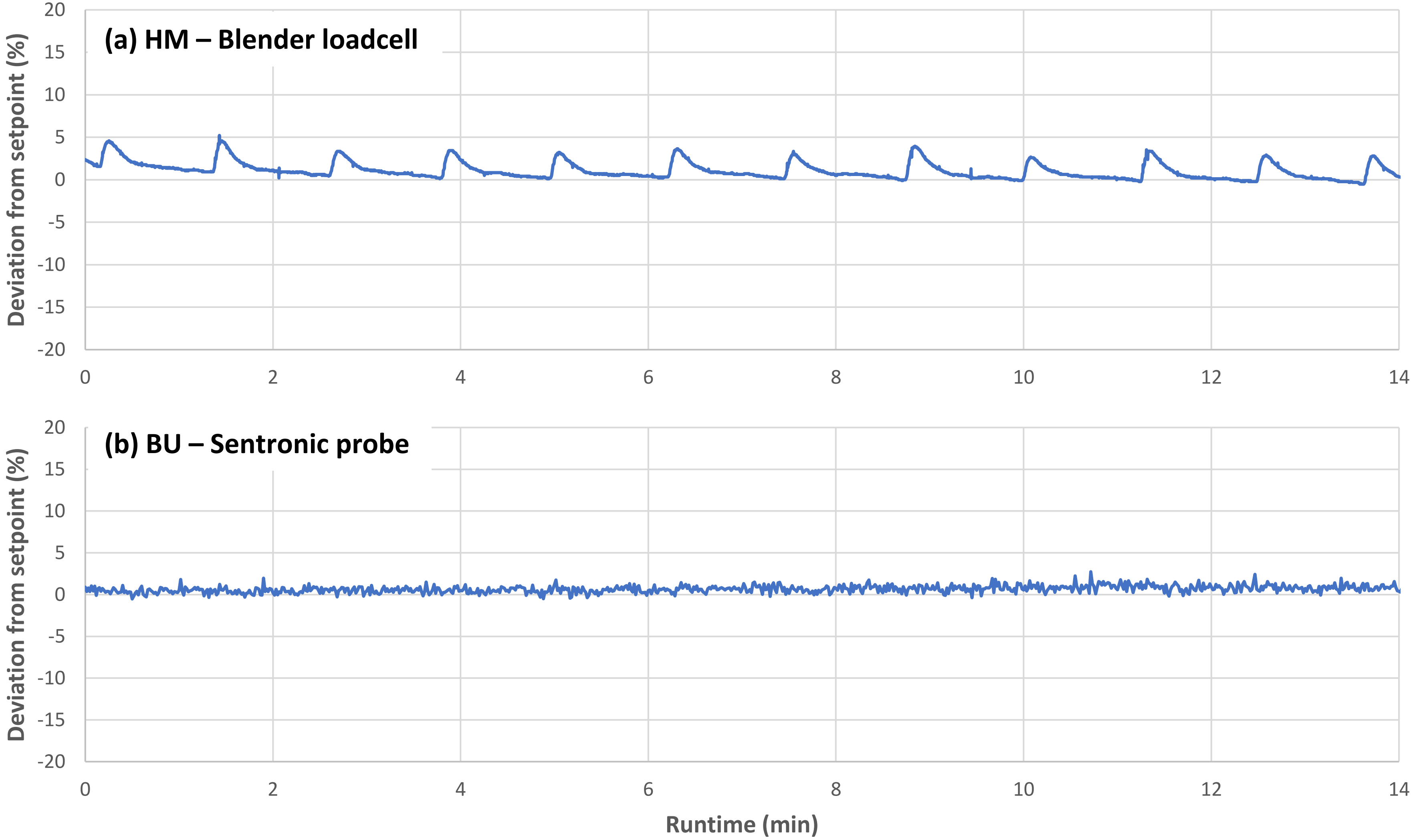

#### 5.4.1.2 Time to steady state

The blender trials revealed that it took significantly longer to reach steady state conditions for the blender hold-up mass (i.e. 5 up to 25 minutes) compared to the API concentration (i.e. 15 to 30 seconds). **Figure 11** displays the hold-up mass and API concentration profiles for a high and low API content blend where target API concentration was reached almost immediately while the hold-up mass was still stabilizing. In **Figure 11a**, the initial peak was caused by the priming step of the feeders. These observations suggest that the blender hold-up mass does not need to be in steady state conditions in order to assure a stable API concentration.

#### 5.4.1.3 BU off-line verification

Off-line UV-VIS analysis was performed on a selection of grab samples taken during the trials. An overview of the tested grab samples with the measured API concentration (i.e. off-line UV-VIS) and corresponding NIR prediction (i.e. on-line Sentronic probe) is given by **Figure 12**. Based on the prediction error from the model (i.e. 0.5 to 1.2%) and the measurement error from UV-VIS (i.e. 0.5 to 6%), similar results were observed for the off- and on-line measurement of most blends. However, some runs (i.e. F1_5_6; F9_10_7 and F9_10_8) showed a significant difference between both measurements which was attributed to a prediction of higher API concentrations by the NIR model. This offset was the result of window fouling (due to dust adhesion to the probe) which artificially increased the concentration of the blend. The window fouling was observed both visually and in the measurement data (i.e. constant values and/or increase in concentration over time). Furthermore, larger deviations from the target were seen for the 5% API blends which originated from the feeders. At low API concentrations, the feeders worked near the lower screw speed limits (i.e. 3% screw capacity) resulting in a less stable mass flow, as was seen in the feeder study by Bekaert et al. (2021).

***Figure 11:*** *Blender hold-up mass and API concentration profiles for (a) F9_70_4 (i.e. 70% T_P at a throughput of 5 kg/h and Froude 8) and (b) F2_5_4 (i.e. 5% P_DP at a throughput of 5 kg/h and Froude 8). API and color spikes, used for the RTD measurements, are marked with a black arrow.*

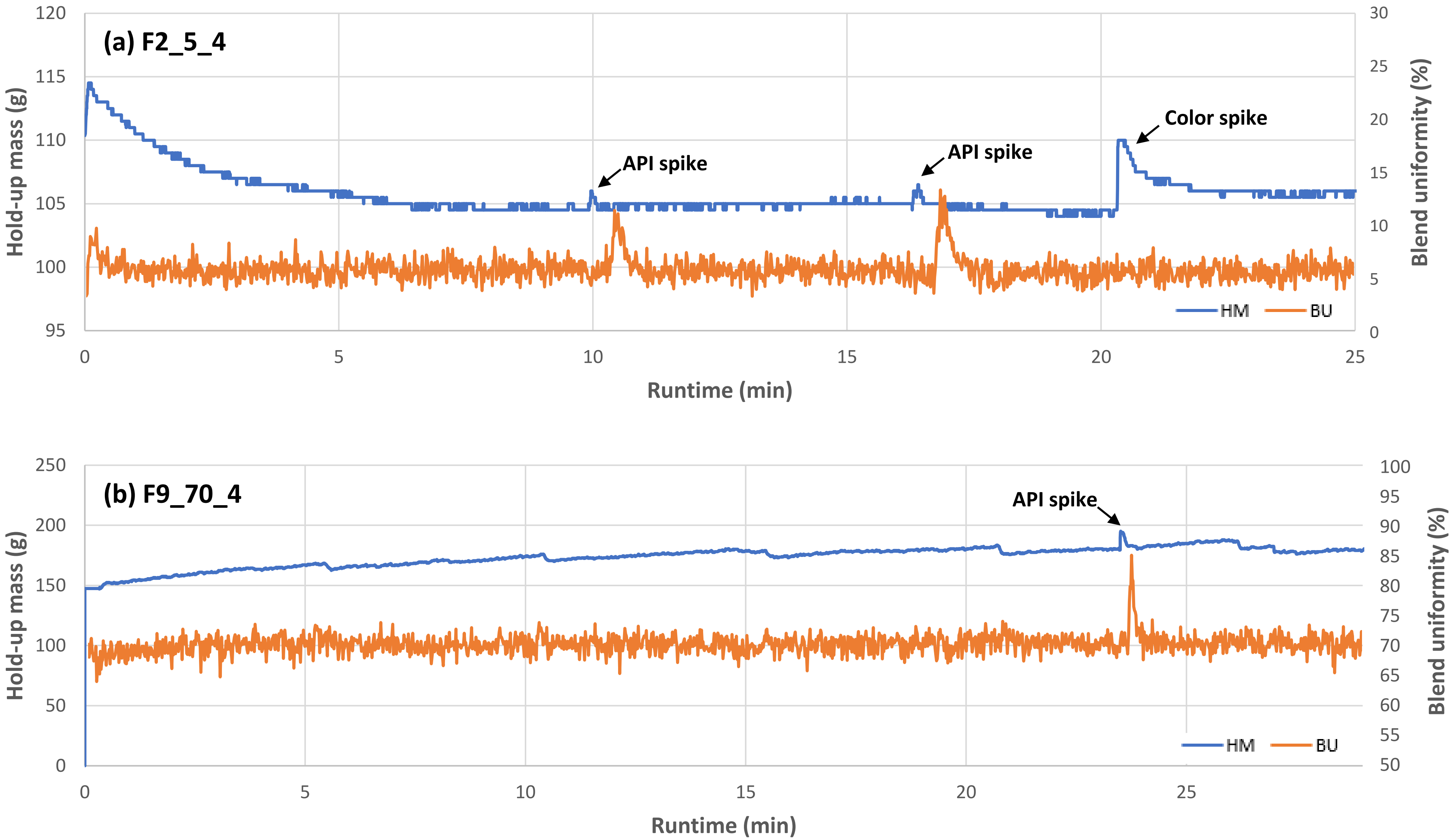

***Figure 12:*** *Comparison between the predicted API concentration measured with the online Sentronic probe and the API concentration measured off-line analysis via UV-VIS. Measurements that showed window fouling are marked with a red square.*

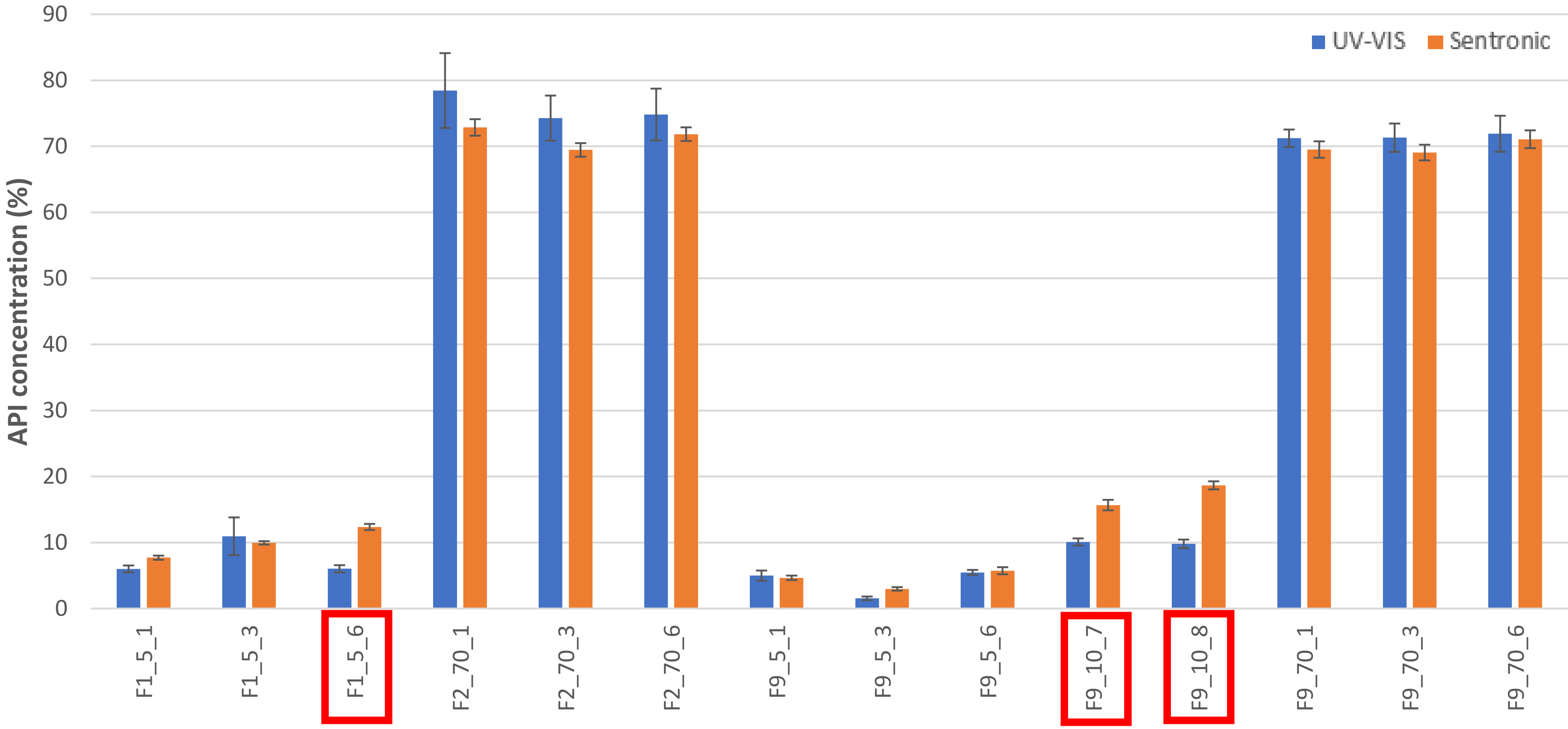

### 5.4.2 Multivariate data analysis

The collected blending responses (i.e. HM, MRT, #BP and $RSD_{BU}$) were included into one overall PLS model with a goodness of fit ($R^2Y$) and prediction ($Q^2$) of 74.4% and 68.4%, respectively. The runs for F3 with 70% API were excluded from the model due to the inability of the feeders to correctly dose the product. Additionally, runs showing window fouling of the NIR probe were excluded from the model. An overview of the $R^2Y$ and $Q^2$ for each principle component and response is given in **Table 8**. The correlations between the blend properties, process settings and blender responses (i.e. HM, MRT, #BP and $RSD_{BU}$) were established using the scores and loadings plots of the overall model (i.e. PC1 vs. PC2 and PC1 vs. PC3; **Figure 13**). To gain better insight in the correlations, coefficient plots were used where positive values for a variable indicate a positive correlation between that variable and the blender response. The significance of these values was determined using a 95% confidence level.

Furthermore, MLR was used to evaluate the significance of the factors and factor interactions from the performed DoE. The application of MLR resulted in coefficient and interaction plots that quantitatively displayed the influence of the factors/factor interactions on each response (i.e. HM, MRT, #BP and $RSD_{BU}$).

***Table 8:*** *Overview of the constructed PLS model for the blender trials. $R^2Y$ and $Q^2$ is given for the principle components and all blending responses.*

| **Overal model** | | |
|---|---|---|
| **#PC** | **$R^2Y$** | **$Q^2$** |
| **1** | 0.219 | 0.200 |
| **2** | 0.683 | 0.621 |
| **3** | 0.744 | 0.684 |
| **Responses** | | |
| **Name** | **$R^2Y$** | **$Q^2$** |
| **HM** | 0.765 | 0.674 |
| **$RSD_{BU}$** | 0.800 | 0.767 |
| **#BP** | 0.667 | 0.591 |

*__Figure 13:__ Overall PLS model for the blender trials: (a) PC 1 vs PC 2 and (b) PC 1 vs PC 3 loadings plot.*

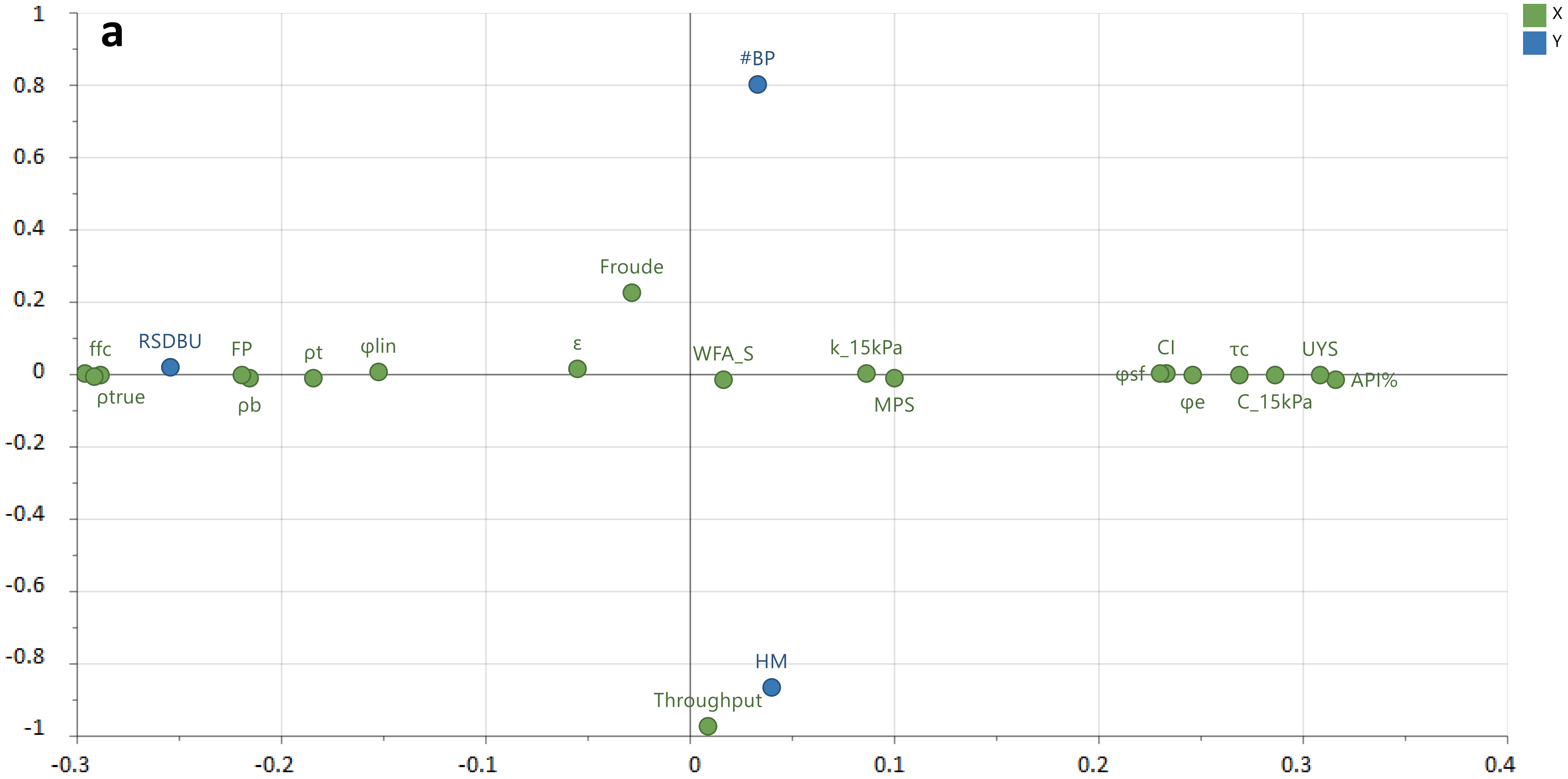

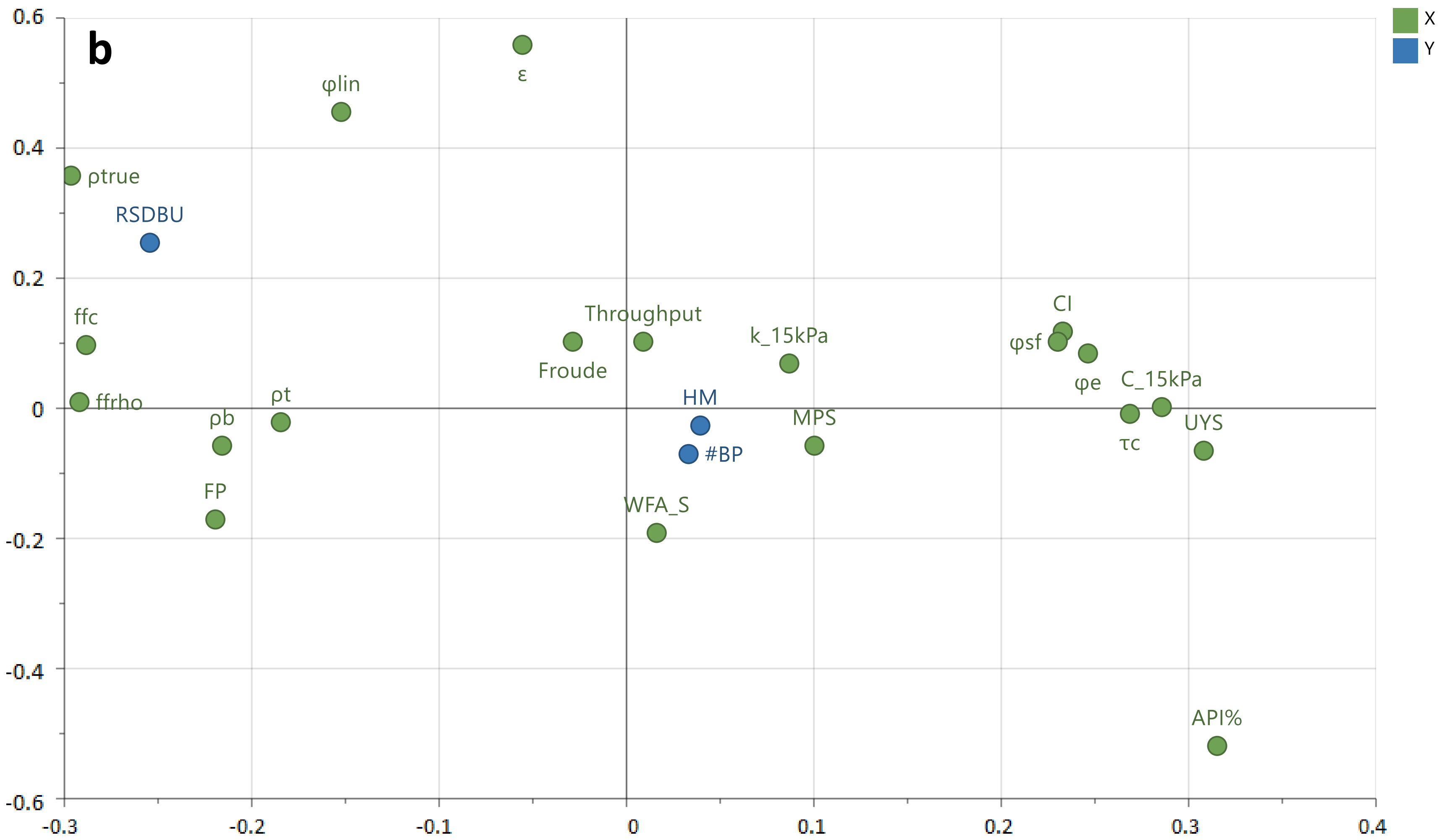
b
X
Y
φlin
ε
ρtrue
RSDBU
ffc
ffrho
ρb
ρt
FP
Throughput
Froude
k_15kPa
HM
#BP
MPS
WFA_S
CI
φsf
φe
C_15kPa
τc
UYS
API%
0.6
0.4
0.2
0
-0.2
-0.4
-0.6
-0.3
-0.2
-0.1
0
0.1
0.2
0.3
0.4

#### 5.4.2.1 Hold-up mass

The PLS model explained 76.5% of the variation in the Y-matrix for the hold-up mass. Looking at the loadings plot for PC1 vs PC2 (**Figure 13a**), both the throughput and HM were located in the same location, indicating a strong positive correlation. Froude number was at the opposite side of the origin, suggesting an inverse correlation with the hold-up mass. While an increase in throughput resulted in more material passing through the blender (i.e. higher HM), a higher Froude number increased the forwarding effect of the impeller configuration, yielding a lower HM. Furthermore, the clear separation of Froude number and throughput (i.e. process settings) from the blend properties (located around the x-axis/PC1) confirmed that there was no correlation between the blend properties and process settings. The loadings plot for PC1 vs PC3 (**Figure 13b**), depicting the correlations between blend properties in more detail, confirmed that there was no influence of blend properties or API ratio (i.e. API%) on the hold-up mass. (i.e. located near the origin).

MLR analysis of the hold-up mass established similar observations (data not shown) as the PLS regression for this specific experimental setup, indicating that the only way to change the hold-up mass, without changing the impeller configuration, was to alter the process settings.

#### 5.4.2.2 API Concentration variability

The descriptor $RSD_{BU}$ was found in the blend property cluster (i.e. along the x-axis) (**Figure 13a**), indicating that there were correlations with the blend properties, but none with the process settings (i.e. throughput and Froude number). The location of the blend properties describing powder flow (i.e. ffc, ff$\rho$, FP) and density ($\rho$b, $\rho$t and $\rho$true) close to the $RSD_{BU}$ on the loadings plot for PC1 vs PC3, (**Figure 13b**), implied a positive correlation. The positive influence of the better powder flowability could be attributed to a decrease in axial dispersion (i.e. back-mixing) of the blend (Vanarase et al., 2013). There was less resistance for the impeller paddles to pass through a good flowing blend, reducing the effect of the paddles on the powder bed. Therefore, powder movement was mainly impacted by the pushing effect of the powder in the blender, resulting in less forward or reverse flow potential. Consequently, this suggests that the blend showed inconsistent axial and radial mixing which resulted in a higher variability in the blend composition (i.e. higher $RSD_{BU}$). Furthermore, a cluster describing the blend cohesivity and compressibility was located at the opposite side of the origin, confirming the inverse correlation of a poorly flowing blend. The influence of the compressibility was due to a higher paddle interaction of a highly compressible powder, thus increasing the mixing potential (i.e. lower $RSD_{BU}$). The positive contribution of density was related to the blender fill level. At a specific throughput, dense mixtures had a lower volume of material in the blender compared to less dense mixtures, decreasing the paddle interaction. The reduction in paddle interactions, decreased the mixing potential and mixing consistency, resulting in a higher $RSD_{BU}$. However, dedicated experiments are required to confirm the impact of blender fill level on the mixing potential. Additionally, a clearly negative correlation with the API content (i.e. API%) was observed. A higher API content increased the cohesivity of the blend as most APIs were more cohesive compared to the fillers, generating a higher and more consistent mixing potential. Another reason for the decrease in variability was attributed to the normalization of the standard deviation (SD) by a higher mean API percentage for blends with a higher API content.

Similar to the HM analysis, MLR confirmed the PLS observations.

**5.4.2.3 Mean residence time**

Mean residence time was not included into the overall PLS model due to a significant decrease in goodness of fit ($R^2Y$) and prediction ($Q^2$) (i.e. from 74.4% to 59% and 67.4% to 51.9%, respectively), resulting in a lower predictive performance of the model. Therefore, no conclusions or predictions were made with the PLS model.

Multiple linear regression of the MRT data elucidated the significance of the throughput, Froude number and blend flowability (i.e. t1) on the mean residence time (**Figure 14**). The influence of the throughput and Froude number confirmed the observations seen during the preliminary trials with the weir plate. An increase in throughput resulted in a higher HM. The larger amount of powder created a higher driving force to push the material through the blender, resulting in a shorter MRT. This was also achieved at higher impeller speed (i.e. Froude number). The longer MRT due to a better blend flowability was caused by the lower resistance of the blend to the passing impeller paddles. Consequently, the paddles passed through the good flowing powder without generating the forward pushing effect, extending MRT. Furthermore, an interaction between throughput and t1 was observed where the throughput was the determining factor. The enhanced pushing effect when changing the throughput had a bigger impact on MRT (i.e. decrease) than the blend flowability.

*__Figure 14:__ Full factorial DoE: coefficient plot for the mean residence time. Significance was determined using a 95% confidence interval.*

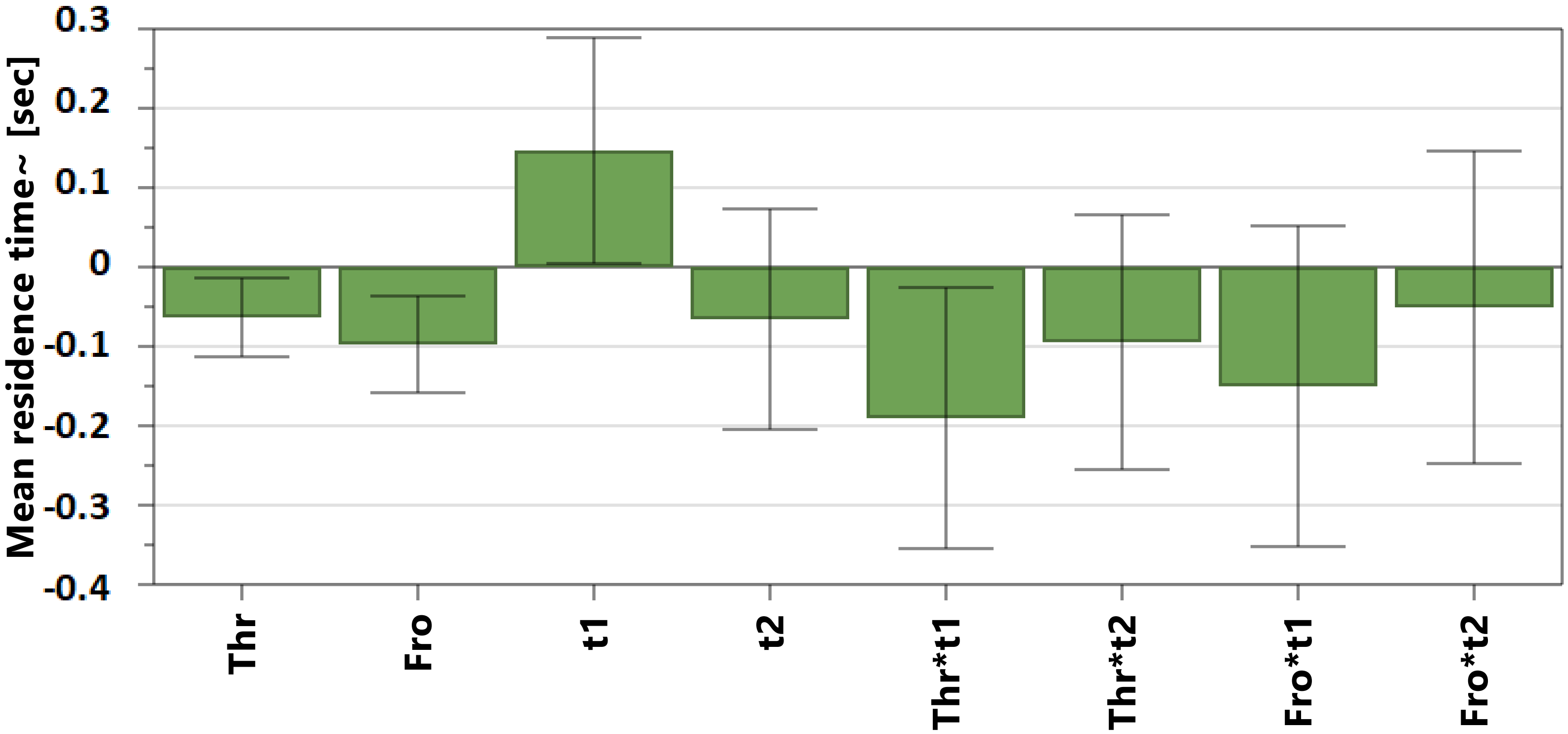

#### 5.4.2.4 Number of blade passes

The location of the descriptor #BP in the loadings plot for PC1 vs PC2 (**Figure 13a**) indicated an anti-correlation with the hold-up mass and throughput. A higher throughput resulted in a lower mean residence time, hence the powder is exposed to less blade passes. While the impeller speed (i.e. Froude number) was positively correlated with #BP, its impact was smaller due to the negative effect of the impeller speed on the mean residence time. Furthermore, a clear separation of #BP from the blend property cluster on the loadings plot was seen, illustrating that there was no correlation with the blend properties.

The analysis of the #BP via MLR established the same observations as seen through PLS, confirming that, for the current setup, the #BP could only be altered through a change in process settings.

### 5.5 Impeller configuration evaluation

As was seen during the blender trials, a change in impeller configuration could potentially improve the blend processability as this can affect the blending responses (i.e. MRT, HM and $RSD_{BU}$). An evaluation of the responses is given in **Table 6**.

To improve the mixing potential of the blender in order to reduce the $RSD_{BU}$ without significantly changing HM or MRT, the paddle angle can be modified from axial (i.e. forward paddles = +20°; backward paddles = -20°) to radial (i.e. forward paddles = +70°; backward paddles = -80°) (**Figure 6**; **Configuration 2**). The radial paddles introduced intense radial mixing zones, compared to the axial back-mixing from the turbulent mixing zones. Adding more backward paddles as well as increasing the size of the back-mixing zones (i.e. from 2 to 3 backward paddles per zone) (**Configuration 3**) also significantly reduced $RSD_{BU}$. This configuration prolonged the material residence time in the blender, allowing more back-mixing. On the other hand, it resulted in a higher hold-up mass, a longer MRT and a longer time to reach steady state conditions for the hold-up mass.

Blending processes that show an optimal blending performance could benefit from a reduction in blending time (i.e. MRT). A reduction in MRT could be achieved by replacing some backward pushing paddles by forward pushing paddles (**Configuration 4**). The additional forwarding effect reduced MRT of the blend drastically with only a limited drop in HM. A disadvantage of a shorter blending time could be the limited time to decrease/remove any deviations (i.e. higher $RSD_{BU}$).

**Configuration 5** combined an initial forward pushing zone with radial forward and backward paddles. The initial pushing effect on the blend, combined with the more intense radial mixing in the next zones, reduced $RSD_{BU}$, MRT and HM. Moreover, depending on the impeller speed, $RSD_{BU}$ and MRT could be varied. At low Froude number, higher MRT and lower $RSD_{BU}$ values were observed, while at high Froude number MRT was shorter in combination with a higher $RSD_{BU}$.

## 6. Conclusion

This study established a quantitative relationship between blend properties, process settings and blending responses via multivariate data analysis (i.e. MLR and PLS). For the studied impeller design, the analysis elucidated a clear correlation between the process settings (i.e. throughput and Froude number) and the blending responses describing the blender hold-up mass, mean residence time and number of blade passes. Furthermore, the blend properties only contributed to the mean residence time and $RSD_{BU}$, with flowability, compressibility and blend density as the most important properties. The weir plate trials and impeller configuration evaluations pointed out that the blender performance could be optimized through a change in impeller configuration, whereas the addition of a weir plate showed no added value. The blender with its standard impeller configuration was successful in dampening short/small feeder fluctuations, which are inherently present during long term LIW feeding. However, the standard impeller configuration was not able to dampen long/large feeder deviations, which significantly impacted BU. In order to cope with such deviations and increase the blender performance, a change in impeller configuration and/or optimization of the feeding process is required, emphasizing the need for further dedicated experiments. Furthermore, the blender trials elucidated that the blender hold-up mass does not need to be in steady state conditions in order to assure a stable API concentration. The latter finding could make a paradigm shift in production, re-defining the start-up conditions (i.e. minimize start-up loss) and allowing earlier start of a continuous production campaign (i.e. shorter production shifts). Overall, this study demonstrated the generic application of this blender where the standard impeller configuration could be used for processing a wide range of binary blends, while the developed PLS models could be used to predict the blender performance based on the characterization of the blend properties. When including impeller configurations, this platform could eventually suggest optimized blender settings for a specific formulation in order to tailor the blending process in silico.

**Acknowledgments**

This work was supported by the agency Flanders Innovation and Entrepreneurship (Project n° HBC.2018.0135) and Fette Compacting. Brabender and Fette Compacting Belgium are acknowledged for kindly providing support during the project.

## References


B. Bekaert, L. Penne, W. Grymonpré, B. Van Snick, J. Dhondt, J. Boeckx, J. Vogeleer, T. De Beer, C. Vervaet, V. Vanhoorne, 2021. Determination of a quantitative relationship between material properties, process settings and screw feeding behavior via multivariate data-analysis. Int. J. Pharm. 602. https://doi.org/10.1016/j.ijpharm.2021.120603

Bostijn N, Dhondt J, Ryckaert A, Szabó E, Dhondt W, Van Snick B, et al. A multivariate approach to predict the volumetric and gravimetric feeding behavior of a low feed rate feeder based on raw material properties. Int J Pharm [Internet]. 2019;557(December 2018):342–53. Available from: https://doi.org/10.1016/j.ijpharm.2018.12.066

Engisch WE, Muzzio FJ. Loss-in-Weight Feeding Trials Case Study: Pharmaceutical Formulation. J Pharm Innov. 2014;10(1).

Engisch, W., Muzzio, F., 2015a. Using Residence Time Distributions (RTDs) to Address the Traceability of Raw Materials in Continuous Pharmaceutical Manufacturing. J. Pharm. Innov. 11, 64–81. https://doi.org/10.1007/s12247-015-9238-1

Ervasti T, Simonaho SP, Ketolainen J, Forsberg P, Fransson M, Wikström H, et al. Continuous manufacturing of extended release tablets via powder mixing and direct compression. Vol. 495, International Journal of Pharmaceutics. 2015. p. 290–301.

Fogler, S., 2006. Elements Of Chemical Reaction Engineering., Fourth. ed. Pearson international.

Gao, Y., Vanarase, A., Muzzio, F., Ierapetritou, M., 2011. Characterizing continuous powder mixing using residence time distribution. Chem. Eng. Sci. 66, 417–425. https://doi.org/10.1016/j.ces.2010.10.045

Ierapetritou, M., Muzzio, F., Reklaitis, G., 2016. Perspectives on the continuous manufacturing of powder-based pharmaceutical processes. AIChE J. 62, 1846–1862. https://doi.org/10.1002/aic.15210

Järvinen, K., Hoehe, W., Järvinen, M., Poutiainen, S., Juuti, M., Borchert, S., 2013a. In-line monitoring of the drug content of powder mixtures and tablets by near-infrared spectroscopy during the continuous direct compression tableting process. Eur. J. Pharm. Sci. 48, 680–8. https://doi.org/10.1016/j.ejps.2012.12.032

Järvinen, M.A., Paaso, J., Paavola, M., Leiviskä, K., Juuti, M., Muzzio, F., Järvinen, K., 2013b. Continuous direct tablet compression: effects of impeller rotation rate, total feed rate and drug content on the tablet properties and drug release. Drug Dev. Ind. Pharm. 39, 1802–8. https://doi.org/10.3109/03639045.2012.738681

K. Marikh, H. Berthiaux, V. Mizonov, E. Barantseva, D. Ponomarev, Flow analysis and Markov chain modelling to quantify the agitation effect in a continuous powder mixer, Chemical Engineering Research and Design 84 (2006) 1059–1074.

Osorio, J.G., Muzzio, F.J., 2016. Effects of processing parameters and blade patterns on continuous pharmaceutical powder mixing. Chem. Eng. Process. Process Intensif. Volume 109, 59–67.

Pernenkil, L., Cooney, C.L., 2006. A review on the continuous blending of powders. Chem. Eng. Sci. 61, 720–742. https://doi.org/10.1016/j.ces.2005.06.016

Portillo, P.M., Ierapetritou, M.G., Muzzio, F.J., 2008. Characterization of continuous convective powder mixing processes. Powder Technol. 182, 368–378. https://doi.org/10.1016/j.powtec.2007.06.024

Rogers A, Hashemi A, Ierapetritou M. Modeling of Particulate Processes for the Continuous Manufacture of Solid-Based Pharmaceutical Dosage Forms. Processes. 2013;1(2):67–127.

Simonaho, S.-P., Ketolainen, J., Ervasti, T., Toiviainen, M., Korhonen, O., 2016. Continuous manufacturing of tablets with PROMIS-line - Introduction and case studies from continuous feeding, blending and tableting. Eur. J. Pharm. Sci., Volume 90, 2016, Pages 38-46, ISSN 0928-0987 https://doi.org/10.1016/j.ejps.2016.02.006

Van Snick, B., Holman, J., Vanhoorne, V., Kumar, A., De Beer, T., Remon, J.P., Vervaet, C., 2017b. Development of a continuous direct compression platform for low-dose drug products. Int. J. Pharm. 529. https://doi.org/10.1016/j.ijpharm.2017.07.003

Van Snick, B., Holman, J., Cunningham, C., Kumar, A., Vercruysse, J., De Beer, T., Remon, J.P., Vervaet, C., 2017a. Continuous direct compression as manufacturing platform for sustained release tablets. Int. J. Pharm. 519. https://doi.org/10.1016/j.ijpharm.2017.01.010

Van Snick, B., Dhondt, J., Pandelaere, K., Bertels, J., Mertens, R., Klingeleers, D., Di Pretoro, G., Remon, J.P., Vervaet, C., De Beer, T., Vanhoorne, V., 2018. A multivariate raw material property database to facilitate drug product development and enable in-silico design of pharmaceutical dry powder processes. Int. J. Pharm. 549, 415–435. https://doi.org/10.1016/j.ijpharm.2018.08.014

Van Snick B, Kumar A, Verstraeten M, Pandelaere K, Dhondt J, Di Pretoro G, et al. Impact of material properties and process variables on the residence time distribution in twin screw feeding equipment. Int J Pharm. 2019;556:200–16.

Van Snick B. Experimental and model-based analysis of a continuous direct compression platform for oral solid dosage manufacturing. [Ghent, Belgium]: Ghent University. Faculty of Pharmaceutical Sciences; 2019 http://hdl.handle.net/1854/LU-8610640

Vanarase, A. U., & Muzzio, F. J. (2011). Effect of operating conditions and design parameters in a continuous powder mixer. Powder Technology, 208(1), 26–36. https://doi.org/10.1016/j.powtec.2010.11.038

Vanarase, A. U., Osorio, J. G., & Muzzio, F. J. (2013). Effects of powder flow properties and shear environment on the performance of continuous mixing of pharmaceutical powders. Powder Technology, 246, 63–72. https://doi.org/10.1016/j.powtec.2013.05.002

Zeki Berk, Oldshue JY. Mixing. Ind Eng Chem. 1967;59(11):58–70. https://doi.org/10.1016/B978-0-12-373660-4.00007-7